

Study of Near UV Light-Emitting Diodes Based on Intentionally Doped ZnO Nanoparticles

A dissertation submitted in partial fulfilment of
the requirements for the degree of

Doctor of Philosophy

By

ISLAM MOHAMMAD SHAFIQL

Supervisor:

Professor Dr. Yasuhisa Fujita

Assistant Supervisor:

Professor Dr. Yasuji Yamada

Professor Dr. Ryo Sasai

Associate Professor Dr. Wenchang Yeh



Collaborative Course in Science and Engineering
Interdisciplinary Graduate School of Science and Engineering

Shimane University, Japan

March 2022

Table of Contents

Abstract of the dissertation	6
1. Introduction	7
1.1 Introduction to Light Emitting Diodes (LEDs)	7
1.2 Introduction to ZnO materials-based LEDs	8
1.3 Introduction to ZnO nanoparticle-based LEDs	11
1.4 Organize the dissertation	13
2. Preparation and Characterization of ZnO Nanoparticles	15
2.1 Preparation Method	15
2.2 Characterization	17
2.2.1 Raman Spectroscopy	17
2.2.2 Nitrogen concentrations and Raman peak ($275, 581 \text{ cm}^{-1}$) Intensity	20
2.2.3 X-ray diffraction	22
2.2.4 PL	25
3. Fabrication and characterization of ZnO: N NPs (p)/ GZO UV LEDs	29
3.1 Fabrication of LEDs	29
3.2 <i>I-V</i> characterization	30
3.3 EL	31
3.4 Conclusion	33
4. Fabrication and characterization of ZnO: N NPs(p)/ZnO: Ga NPs (n)/GZO homo-junction UV LEDs	34
4.1 Materials preparation	34
4.2 X-ray diffraction of as-prepared ZnO NPs and Ga-doped ZnO NPs	36
4.3 PL Comparison	37
4.4 Hall measurement for ZnO NPs	40
4.5 Fabrication of LEDs	41
4.6 SEM measurement	43
4.7 <i>I-V</i> characteristics and light output power measurement	45
4.8 EL	46
4.9 Conclusion	50



5. The hetero-structure LEDs based on ZnO NPs by inserting ZnMgO NPs layer	51
5.1 ZnMgO composite NPs preparation	52
5.2 X-ray diffraction	53
5.3 Optical absorption	54
5.4 PL	55
5.5 Devices fabrication	56
5.6 <i>I-V</i> Characteristics	58
5.7 EL	59
5.8 Conclusion	62
6. Summary	63
7. Future Task	65
Reference	66
List of Publications	76
Acknowledgments	78

List of Figures

Figure 1. The mechanism of LEDs.

Figure 2. The Schematic view of p-type and n-type ZnO nanoparticle-based LEDs and EL emission.

Figure 3. Schematic view of DC Arc Plasma Gas Evaporation system (MODEL: GE-970).

Figure 4. Optical phonon modes of wurtzite ZnO. The polar phonon modes A_1 and E_1 split into LO and TO. The B_1 and E_2 are non-polar modes.

Figure 5. The Raman Spectrum of ZnO NPs (The preparation condition of ZnO NPs was at the arc current of 30 A and the chamber pressure condition of 75 ~ 760 Torr).

Figure 6. The Raman Spectrum of ZnO NPs (The preparation condition of NPs was at the chamber pressure condition of 150 Torr and the arc current of 20 ~ 70 A).

Figure 7. Nitrogen concentration of ZnO NPs as a function of arc current (20 A ~ 70 A).

Figure 8. The Raman peak intensity (275 cm^{-1} and 582 cm^{-1}) (dot line) and nitrogen concentration (solid line) as a function with the arc current condition of 20 ~ 70 A.

Figure 9. The hexagonal structure of ZnO with wurtzite crystal.

Figure 10. X-ray diffraction of N-doped p-type ZnO NPs.

Figure 11. PL emission spectra of N-doped p-type ZnO NPs (The preparation condition of NPs was at the chamber pressure condition of 150 Torr and the arc current of 20 ~ 70 A).

Figure 12. (a) is the Gaussian deconvolution for NBE emission of PL spectra of N-doped p-type ZnO NPs; (b) is the ratios of DAP / Exciton emission versus Raman peak 275 cm^{-1} intensity

Figure 13. The schematic view of ZnO-based LEDs.

Figure 14. *I-V* characterization of ZnO NPs based LEDs.

Figure 15. (a) The EL spectra of ZnO NPs LEDs (Inset shows the UV emission of LEDs). The graph of EL intensity of LEDs versus DAP / Exciton emission (b) and Raman peak intensity of p-type ZnO NPs (c).

Figure 16. The preparation process of Ga-doped ZnO NPs using thermal ambient.

Figure 17. X-ray diffraction spectra of the as-prepared ZnO NPs and Ga-doped ZnO NPs. The inset shows a comparison of the diffraction peak (002) for the as-prepared ZnO NPs and Ga-doped ZnO NPs.

Figure 18. PL spectra of the as-prepared ZnO NPs (solid line) and Ga-doped ZnO NPs (dot line) sprayed layers.

Figure 19. PL emission spectra for N-doped p-ZnO NPs (solid line) and Ga-doped n-ZnO NPs (dot line).

Figure 20. Schematic diagram of ZnO NPs based LEDs. (a) p-ZnO NPs/GZO structure (b) p- ZnO NPs/n-ZnO NPs/GZO structure.

Figure 21. SEM surface image of the ZnO NP layers (a); particles size of the ZnO NPs (b); SEM cross section images p-ZnO NP layer (c), p-ZnO NP layer and n-ZnO NP layer (d).

Figure 22. *I-V* characterization and EL power of ZnO NPs based LEDs with the structure of p-ZnO/n-ZnO/GZO and p-ZnO/GZO.

Figure 23. Comparison of EL spectra for ZnO NPs LEDs with the structure of p-ZnO/n-ZnO/GZO and p-ZnO/GZO. The LED's UV emission photographs show in the insets with the forward bias of 10 V.

Figure 24. Comparison of EL spectra for ZnO NPs LEDs with the structure of p-ZnO/n-ZnO/GZO at the injection currents of 40 mA and 200 mA.

Figure 25. The preparation process of ZnMgO composite NPs using thermal treatment.

Figure 26. X-ray diffraction of as-prepared ZnO NPs and ZnMgO composite NPs.

Figure 27. The absorbance of as-prepared ZnO NPs and ZnMgO composite NPs.

Figure 28. Photoluminescence of as-prepared ZnO NPs and ZnMgO composite NPs

Figure 29. Schematic diagram of ZnO NPs based LEDs. (a) p-ZnO NPs/GZO structure (b) p- ZnO NPs/n-ZnMgO NPs/GZO structure.

Figure 30. The band diagram of ZnO NPs based LEDs (band bending is not taken into account) (a) p-ZnO/GZO structure; (b) p- ZnO/n-ZnMgO/GZO structure.

Figure 31. *I-V* characterization of ZnO NPs based LEDs with the structure of p-ZnO/n-ZnMgO/GZO and p-ZnO/GZO.

Figure 32. Comparison of EL spectra for ZnO NPs LEDs with the structure of p-ZnO/n-ZnMgO/GZO and p-ZnO/GZO.

Figure 33. The band diagram of ZnO NPs based LEDs at forward bias condition (band bending is not taken into account) (a) p-ZnO/GZO structure; (b) p- ZnO/n-ZnMgO/GZO structure.

Abstract of the dissertation

In this study, nitrogen-doped ZnO nanoparticles were synthesized, and homojunction and heterojunction light-emitting diodes were fabricated to discuss the nitrogen-induced p-type conduction and carrier behavior.

The synthesis of nitrogen-doped ZnO nanoparticles was carried out by the DC arc plasma gas evaporation method. The influence of nitrogen incorporation has been investigated with the local vibrational modes of Raman spectra. The structural and optical emission properties were studied by X-ray diffraction and photoluminescence, respectively. The nitrogen concentration of the ZnO nanoparticles was determined from the results of the intensity of the Raman peak at 275 cm^{-1} , which is linearly proportional to the intensity of donor-acceptor pair recombination estimated from photoluminescence spectra. Nitrogen-doped ZnO nanoparticles were demonstrated as a p-type hole transport layer used to fabricate light-emitting diodes. The intensities of electroluminescence of these devices were near proportional to the local vibrational mode of Raman spectra and donor-acceptor pair emission of ZnO nanoparticles, which indicates the nitrogen dopants in the ZnO nanoparticles were acting as an acceptor.

The world's first homo-junction UV light-emitting diodes were demonstrated based on p-type and n-type ZnO nanoparticles. Nitrogen-doped ZnO and gallium-doped ZnO nanoparticles were used to fabricate the p-type and n-type nanoparticles layer, respectively. The evaluation of *I-V* characteristics and electroluminescence of the light-emitting diodes confirmed that the holes injected from the p-ZnO nanoparticle layer to the n-ZnO nanoparticle layer and the mechanism of these devices are that of p-n junction light-emitting diodes.

ZnMgO composite nanoparticles were prepared by thermal diffusion of Mg into ZnO nanoparticles and demonstrated heterojunction light-emitting diodes. It can be seen that the addition of the n-ZnMgO NPs layer reduces the leakage current of the light-emitting diode and improves the emission intensity. This is considered due to the hetero-barrier's carrier confinement effect.

1. Introduction

1.1 Introduction to Light Emitting Diodes (LEDs)

In the illumination technology era, light-emitting diodes (LEDs) as semiconductor devices have extensive potential use in solid-state lighting for their high efficiency, low power consumption, low heat output, and long lifetime, which has changed many away from our lives. The transfer from traditional light bulbs and tube lights to LEDs is currently undergoing a revolution. The fluorescent tubes and light bulbs replaced with LEDs will reduce electricity consumption in industrial economies due to the advantages of LEDs. White LEDs are often based on efficient blue or UV LEDs using exciting phosphor material. By combining the multiple colours (red, green, and blue), white LEDs can be created. The blue or UV LEDs have versatile platforms for electronic devices and biomedical applications such as phototherapy (newborn baby jaundice). The UV LEDs will be used for water purification in the future because the DNA of bacteria, viruses, and microorganisms may be destroyed by UV light [1]. LEDs have been widely applied for various optoelectronic applications such as lighting, mobile appliances, automotive, and display due to their luminescence efficiency [2], [3].

The fundamental mechanism of the LED is the emission of the p-n junction[4], [5]. The p-n junction consists of electrons (n-type) and holes (p-type) as carriers for semiconductor materials. At the forward bias voltage, the recombination of electrons and holes occurs around a p-n junction. The light emission wavelength of LEDs depends on the materials and their bandgap energy. **Figure 1** shows how a LED works.

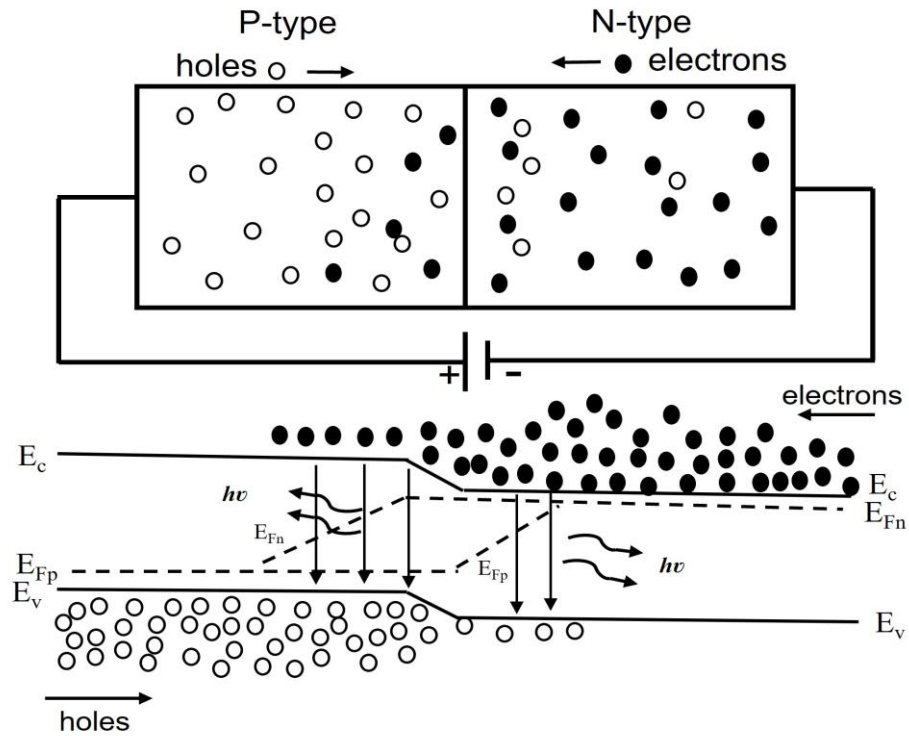


Figure 1. The mechanism of LEDs. Where, E_c is conduction band energy, E_v is valence band energy and quasi- Fermi level energy is E_{Fn} for n-type and E_{Fp} for p-type.

1.2 Introduction to ZnO materials-based LEDs

The improvement of solid-state lighting devices depends on direct bandgap materials like GaN and ZnO. The direct band material GaN has the bandgap energy of 3.44 eV and the exciton binding energy of 25 meV. On the other hand, ZnO as a semiconductor [6] is currently in great interest, which has advantages with a wide bandgap of 3.37 eV, a stable exciton binding energy of 60 meV for near UV spectral range light emission at room temperature, higher electron mobility and thermal conductivity [7]–[9].

ZnO is a naturally n-type conductivity semiconductor. The reason is donor or acceptor behavior defects in ZnO such as oxygen vacancy (V_o), zinc interstitial (Zn_i), etc., and few candidate shallow acceptors [6]. For reliable intentional n-type conductivity of ZnO, donor

impurities can be used. The group III elements (B, Al, Ga, and In) are more suitable for n-type doping of ZnO compared to other group elements. Group III elements act as shallow donors and substitute on the Zn site [10]–[13]. There are various deposition methods such as MBE (Molecular Beam Epitaxy), PLD (Pulsed Laser Deposition), sputtering, and CVD (Chemical Vapor Deposition) for producing high conductivity n-type ZnO films.

The major issue is controlling the conductivity and achieving p-type ZnO [14], which is strongly related to the device applications. For the tendency of n-type conductivity of ZnO due to low-energy native defects, such as Zn_i or V_o , it is very complicated to obtain p-type conductivity in ZnO. There has no procedure to achieve reproducible and stable p-type ZnO because p-type conductivity in ZnO shows instability, reverting to an n-type conductivity, low solubility in the host material, and few candidates of the shallow acceptor. The most reliable acceptor doping impurities for p-type ZnO are group V elements such as phosphorus (P) [15], arsenic (As), antimony (Sb) [16], [17], and nitrogen (N). Among the acceptor impurities, nitrogen (N) is the most suitable p-type dopant in ZnO due to its closest ionic radius (1.68 Å) to oxygen ionic radius of 1.38 Å. The nitrogen incorporation in ZnO has been reported by several groups, such as N-dopants [18]–[21] and co-dopant with other materials [22]. Fujita et al. [23] reported N-doped ZnO film by MOVPE and investigated N-doped epitaxial films (mobility of 150 cm²/Vs) with high resistivity. However, it is difficult to make stable p-type ZnO films. It was found that the p-type islands are partly distributed in the plane of the nitrogen-doped layer. This makes it impossible to estimate the p-type property by using conventional Hall effect measurements. The reason for the instability of single-crystal films is unknown, but it is thought that the strain in the films will be related to this issue.

LEDs based on GaN are mainly used for various applications such as lighting and display [24]. On the contrary, ZnO has the advantages of useful properties to enable

optoelectronic applications. These beneficial properties of ZnO distinguish from other semiconductors. In addition, ZnO is an abundant and low-cost material as an alternative candidate to GaN. The reason for using ZnO as complementary material to GaN in the optoelectronics sector has conducted researchers worldwide to focus on the advantages of semiconductor properties of ZnO. Researchers suggested that ZnO as a promising material due to large binding energy can be possible to fabricate LEDs by controlling the unintentional n-type conductivity and obtaining the p-type conductivity. Many researchers reported the fabrication of homo-structure and heterostructure LEDs based on ZnO materials. H.C.Chen et al. [25] presented the hetero-junction LEDs using n-ZnO/p-GaN structure. J. Kong et al. [26] fabricated p-type Sb-doped ZnO/ n-type Ga-doped ZnO films on Si (100) substrate-based homo-junction LED. A few researchers investigated nitrogen-doped ZnO or ZnMgO based LEDs with single-crystal films [23], [27]–[29]. As a semiconductor, ZnO has a most attractive features such as the availability of large area single crystal thin film. The epitaxial growth of ZnO thin film can potentially lead high quality with reducing the concentration of extended defects that compare to GaN. The bulk crystal of ZnO can be growth with various techniques, such as MBE [30], [31], CVD [32], sputtering [33], vapor-phase transport [34] and so on.

The single-crystal substrate and the epitaxial growth technologies have the problem of high expenses. The fabrication of LEDs using nanoparticles is facile and inexpensive. This process based on NPs does not need a single-crystal substrate to realize cost-effective semiconductor devices. Most of the making device process can be done in the atmospheric conditions and the vacuum state does not require during the fabrication process. Another advantage is that a large or small surface-emission area can be possible using the manageable methods and it can be mitigated the heating problem of the devices. The nanoparticle films are different from well-known polycrystalline films. Crystal quality in

the nanoparticles synthesized by plasma is good and shows single crystal properties without epitaxial growth. The advantage is stable p-type properties and applicable for a low-cost solution process.

1.3 Introduction to ZnO nanoparticles-based LEDs

Recently, ZnO nanoparticles (NPs) have been a unique and attractive issue. The fabrication of ZnO NPs is grown using different synthesis processes to obtain massive amounts of pure and crystalline nanostructure by controlling particle sizes and structural properties. Previously, many authors developed n-type and p-type conductive ZnO NPs by doping ZnO NPs with donor and acceptor to fabricate LEDs [35]–[37]. To obtain the p-type conductivity of ZnO NPs, nitrogen (N) dopants with ZnO NPs are promising materials. Various fabrication methods were revealed for synthesizing N-doped p-type ZnO NPs by radiofrequency thermal plasma, hydrothermal-ammonolysis, and Nd: YAG laser ablation. [38]–[41]. Our group had successfully developed N-doped ZnO NPs using the gas evaporation method and followed several conditions for obtaining ZnO NPs with p-type conductivity and n-type conductivity [42]–[44]. O. Senthilkumar et al. [43] reported the UV emission from ZnO NPs prepared by a gas evaporation method. K. Senthilkumar et al. [39] presented the mechanism of N-doped ZnO NPs process using the DC arc plasma method and applied these NPs for biomedical application.

Neshataeva et al. [45] presented undoped ZnO NPs-based large area hetero-structure LED using a spin coating method. Al, Ga, Mg, Li doped ZnO NPs as an electron transport layers were used for demonstrating LEDs [36]. On the contrary, our N-doped ZnO NPs show stable p-type behaviour over ten years, and more than a thousand LEDs were fabricated with good reproducibility. We had reported LEDs and TFTs [46] using N-doped ZnO NPs. Itohara et al. [46] presented N-doped p-type and n-type ZnO NPs synthesized

by gas evaporation method and demonstrated the thin-film transistor. Itohara et al. [46] showed the mobility of p-type nanoparticle film was 5~7 cm²/Vs. Those of n-type (undoped) were 0.2~0.7 cm²/Vs. The carrier concentration of p-ZnO NPs film and n-ZnO (undoped) NPs film was $+2.0 \times 10^{12} \sim +2.7 \times 10^{12} \text{ cm}^{-3}$ and $-7.0 \times 10^{15} \sim -5.5 \times 10^{16} \text{ cm}^{-3}$, respectively. Hiragino et al. [38] reported N-doped ZnO NPs prepared by Radio Frequency (RF) thermal plasma and fabricated LEDs based on these NPs. The author Fujita et al. [47] had reported the structure and optical properties of N-doped p-ZnO NPs based LED coated on GZO (Ga-doped ZnO) transparent electrode films. However, previously researcher demonstrated the near-ultraviolet electroluminescence (EL) emission of LEDs using p-ZnO NPs onto the GZO electrode film. The EL emission was detected from the p-type layer of LEDs because GZO film has very weak luminescence and high carrier concentration, where GZO had been used as a n-type layer and acted as a current spreading layer to enhance the injection of electron. On the other hand, it was not understood the role of nitrogen in p-type characteristics of ZnO NPs. In this research, N-doped ZnO NPs were prepared in various conditions by the evaporation method and analysed the material properties depend on the LEDs. The homo-junction UV LED was constructed using N-doped ZnO NPs as a p-type layer and Ga-doped ZnO NPs as a n-type layer. The hetero structure ZnO NPs based LEDs was demonstrated using a ZnMgO composite NPs barrier layer to confine the recombination process. **Figure 2** shows a schematic view of all nanoparticle-based LEDs and EL emission of LEDs.

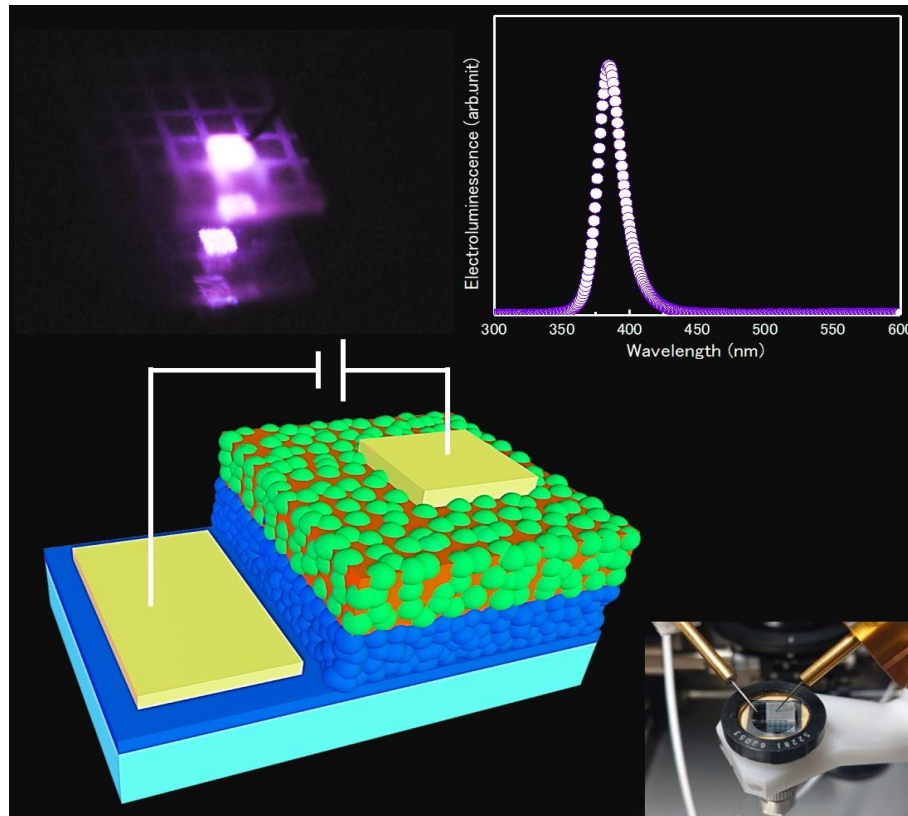


Figure 2. The Schematic view of p-type and n-type ZnO nanoparticle-based LEDs and EL emission (Reference [48]).

1.4 Organize the dissertation

This dissertation is organized based on my research articles [48], [49] and is divided as follows:

1. The DC arc plasma gas evaporation method was studied for the preparation of ZnO NPs. N-doped ZnO NPs was achieved by optimizing the chamber pressure and arc current during the preparation. The nitrogen inclusion in ZnO NPs was confirmed by measuring the Raman spectra, photoluminescence (PL), and X-ray diffraction. The N-doped ZnO NPs as a p-type conductive materials were applied to fabricate

UV LEDs. The UV LEDs were characterized by *I-V* characteristics and EL measurements.

2. To demonstrate UV homo-junction LEDs, N-doped p-type and Ga-doped n-type ZnO NPs were used. The properties of N-doped p-type and Ga-doped n-type ZnO NPs were characterized. It was followed to prepare the LEDs with two different structures (p-ZnO/GZO and p-ZnO/n-ZnO/GZO). These devices were evaluated and compared by measuring the *I-V*, emission power, and EL. It was confirmed that these devices performed as p-n homo-junction UV LEDs.
3. A heterostructure LED with an additional ZnMgO composite NPs layer as an energy barrier in the ZnO NPs LEDs has been realized. The ZnMgO NPs prepared by the composition of ZnO NPs and MgO NPs. The composite ZnMgO NPs layer is inserted in the LEDs' structure (p-ZnO/n-ZnMgO/GZO). The measured characteristics of LEDs with and without the ZnMgO NPs layer of the structure (p-ZnO/ZnMgO/GZO and p-ZnO/GZO) were compared. The results of the LEDs indicated that the reduction of leakage current and the enhancement of the emission were occurred by inserting the ZnMgO NPs layer.

2. Preparation and Characterization of ZnO Nanoparticles

2.1 Preparation Method

ZnO NPs were produced by a vapor gas evaporate deposition method (ULVAC Inc. Model No- GE-970). **Figure 3** shows a schematic diagram of the ZnO NPs generation equipment. It is possible to control inside the chamber of the equipment by changing the conditions of pressure (10 to 760 Torr), arc current (10 to 100 A), and gas flow rate up to 20 Lmin⁻¹. The procedure of the gas evaporation method will be described below.

A zinc (Zn) ingot (Nilaco Corporation- purity 99.99%) was placed as a raw material at a predetermined position inside the chamber. Dry air containing nitrogen and oxygen was supplied to a vacuum state at a constant flow rate. Zn is evaporated continuously by generating arc discharge between the zinc (Zn) ingot and the carbon electrode. At this time, Zn was combined with oxygen (O) in the chamber. ZnO nanostructure powder was generated. The arc discharge is a kind of gas discharge, a phenomenon in which a cathode side is heated by the collision of cations or the like to a very high temperature. A large amount of metal vapor is supplied. Thus, electrons are emitted and discharged from the cathode. As a result, Zn is placed close to the electrode and associated with oxygen in the chamber. In the discharged state, nitrogen (N) in the chamber becomes radical and unstable. So, it becomes an acceptor in ZnO nanoparticles. Therefore, using this facile and manageable method, the generation of p-type ZnO nanoparticles becomes possible.

An arc plasma force and an oxidation system created the preparation of ZnO NPs. The arc plasma generated N₂ radicals to perform nitrogen incorporation in ZnO NPs. The nanoparticles quality depends on the experimental parameters like the chamber pressure, arc current, gas flow rate, and growth period. The chamber pressure throughout the rotary pump and control valve was between 75 Torr to 760 Torr for different conductivity of ZnO



nanoparticles. The implemented arc current was 20 A to 70A between metal zinc anode and carbon cathode. The airflow rate inside the chamber was held at a constant 5 Lmin^{-1} during the synthesis period. In addition, changing the chamber pressure lower to higher makes it possible to generate p-type and n-type conductivity ZnO NPs, respectively. The detailed mechanism of synthesized ZnO NPs described in the previous research report [42], [43].

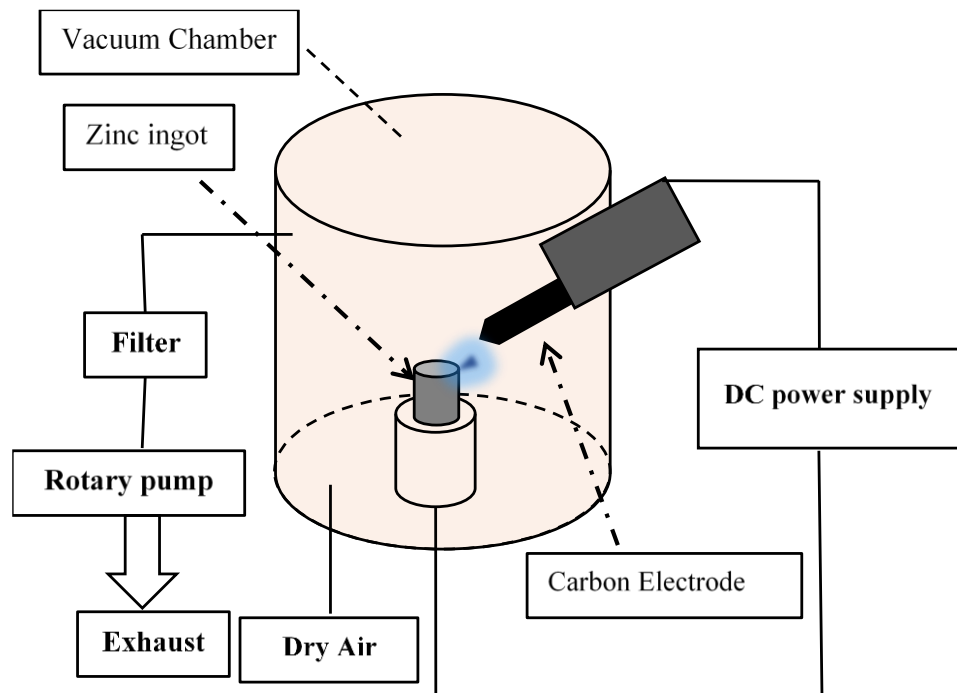


Figure 3. The Schematic view of DC Arc Plasma Gas Evaporation system (MODEL: GE-970).

2.2 Characterization

2.2.1 Raman Spectroscopy

The Raman micro-spectroscopy (Tokyo Instruments Nanofinder 30) with 532 nm laser was used to study fundamental phonons and related impurity-related local vibrational modes. The Raman spectra results confirmed the nitrogen incorporation in prepared ZnO NPs because this measurement process approves to be an excellent method for such study. The wurtzite hexagonal structure ZnO belongs to the symmetry group C_{6v}^4 and consists of the optical phonon modes. The group theory predicts eight sets of phonon normal modes, namely, $2A_1 + 2E_1 + 2B_1 + 2E_2$. The B_1 modes are silent, A_1 and E_1 modes are polar, and Raman active modes. The nonpolar and Raman active E_2 modes have two different frequency modes. The high-frequency E_2 mode involves oxygen atoms, and the low-frequency E_2 mode is associated with the Zn sub-lattice [50]-[52]. **Figure 4** shows the Raman optical phonon modes orientation of wurtzite ZnO.

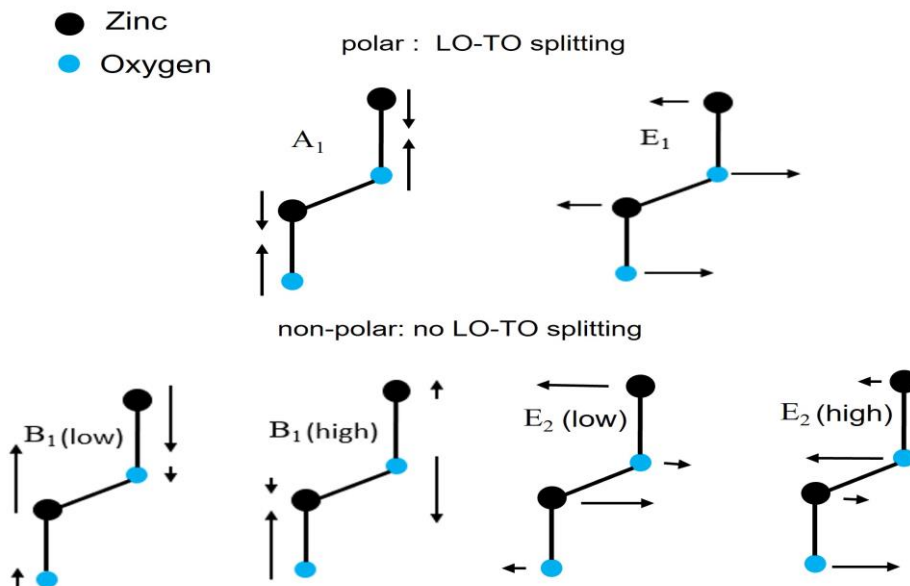


Figure 4. Optical phonon modes of wurtzite ZnO. The polar phonon modes A_1 and E_1 split into LO and TO. The B_1 and E_2 are non-polar modes.

Figure 5 and **Figure 6** display the Raman spectrum results of the produced ZnO NPs that regulated a certain arc current of 30 A with a different chamber pressure of 75 Torr~760 Torr and a particular chamber pressure of 150 Torr with various arc current conditions of 20 A~70 A respectively. According to the Raman spectra of the ZnO NPs, the Raman active non-polar phonon modes E_2 (high) were introduced at 438 cm^{-1} . The polar A_1 (TO) and E_1 (LO) optical modes appeared at 380 cm^{-1} and 584 cm^{-1} , respectively [44], [53]. The 332 cm^{-1} peak intensity of Raman spectra for the second-order scattering feature was attributed to the multi-photon scattering process [54]. In addition, The desired strongest local vibrational modes (LVMS) related on nitrogen content in the Raman spectra were revealed at 275 and 581 cm^{-1} [55] for the possible nitrogen incorporation in the prepared ZnO NPs sample. It was ensured that the additional modes of Raman spectra were according to the disorder imposed by the shallow acceptor dopant. The ZnO NPs synthesized at a constant arc current of 30 A with the chamber pressure of 75 to 760 Torr. In this case, the nitrogen concentration in the ZnO NPs is better at the chamber pressure condition of 150 Torr than the other chamber pressure that indicated the nitrogen related LVM Raman spectrum. The radical of nitrogen lifetime extended at the low chamber pressure throughout fewer collisions, which would improve nitrogen inclusion at O-site in ZnO. On the other hand, the reaction time is shorter at 75 Torr owing to high gas flow inside the chamber and lower nitrogen incorporated than 150 Torr. It was also followed to prepare p-type ZnO NPs at the constant chamber pressure of 150 Torr and different arc currents of 20 to 70 A. In this case, we investigated that the nitrogen related LVM of Raman spectra is better at the arc current of 30 A, comparable to the other arc current conditions.

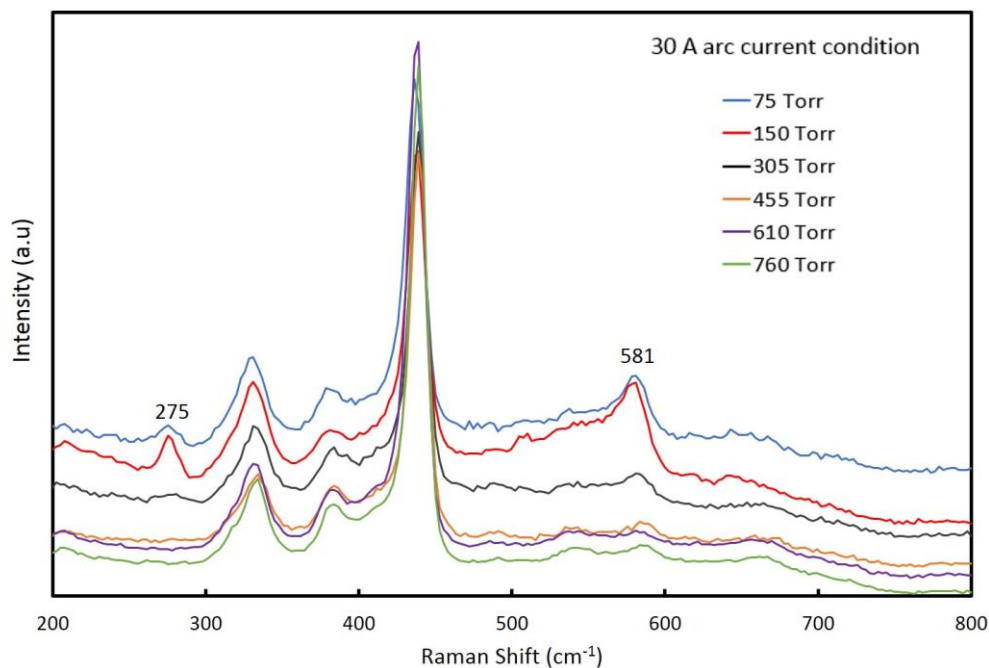


Figure 5. The Raman Spectrum of ZnO NPs (The preparation condition of ZnO NPs was at the arc current of 30 A and the chamber pressure condition of 75 Torr to 760 Torr) (Reference [49]).

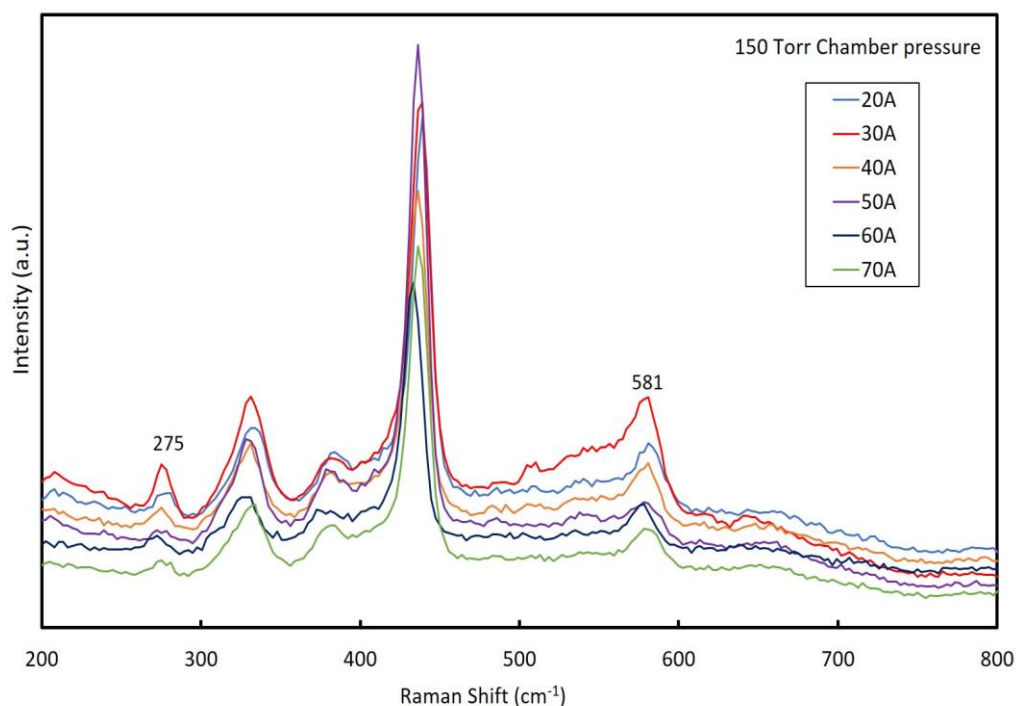


Figure 6. The Raman Spectrum of ZnO NPs (The preparation condition of NPs was at the chamber pressure condition of 150 Torr and the arc current of 20A to 70 A).

2.2.2 Nitrogen concentrations and Raman peak ($275, 581 \text{ cm}^{-1}$) Intensity

The nitrogen concentration of prepared ZnO NP powder samples was measured using a thermal conductivity detector (Horiba EMGA-830). It was followed the condition with a chamber pressure of 150 Torr to prepare ZnO NPs with high nitrogen concentration (approximately $2.6 \times 10^{19} \text{ cm}^{-3}$), which were used to prepare a p-type layer in the LEDs. Low nitrogen concentration (approximately $5.68 \times 10^{18} \text{ cm}^{-3}$) of ZnO NPs were prepared by following at the chamber pressure of 610 Torr. These NPs were used to dope with Ga for preparing high-quality n-type conductivity of ZnO NPs as an n-type layer in the diode. **Figure 7** shows the nitrogen concentration of ZnO NPs at the chamber pressure of 150 Torr and 610 Torr as the function of arc currents of 20 A to 70 A.

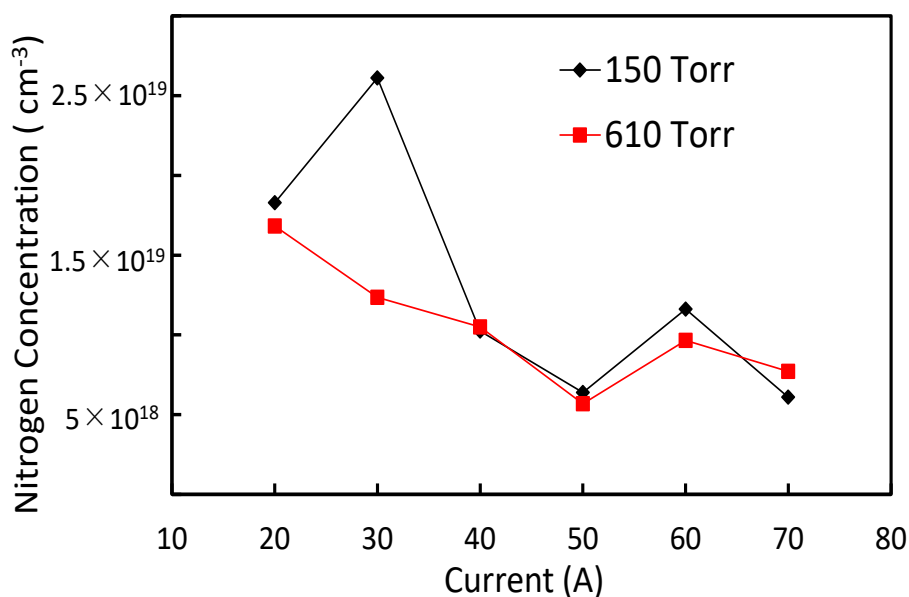


Figure 7. Nitrogen concentration of ZnO NPs as a function of arc current (20 A ~ 70 A).

The relationship between the nitrogen related peaks (275 cm^{-1} and 581 cm^{-1}) of Raman spectra and nitrogen concentration for 150 Torr chamber pressure of ZnO NPs was plotted with arc currents dependency displayed in **Figure 8**. These LVM related peaks of Raman spectra depends on the nitrogen content in the ZnO NPs crystal and found the maximum value at the arc current of 30 A. Because the optimum arc current condition at 30 A enhanced nitrogen concentration in ZnO NPs. The obtained LVM peaks (275 cm^{-1} and 581 cm^{-1}) of Raman spectra value correlate with the measured nitrogen concentration of ZnO NPs. The N-doped ZnO NPs at the arc current condition of 30 A were detected a higher nitrogen concentration of about $2.6 \times 10^{19}\text{ cm}^{-3}$, which was corresponding to the value of nitrogen concentration in N-doped ZnO NPs previously reported [42]. The nitrogen concentration of ZnO NPs measured by the thermal conductivity method contains surface absorbed species of nitrogen molecules. In this case, it can be considered that the prospective value of Raman peak 275 cm^{-1} intensity of ZnO NPs was estimated as the nitrogen concentration of the NPs crystal and detailed in the following discussion. Because the 275 cm^{-1} peaks may have originated from nitrogen substitute at oxygen site, whereas the broad peak at 581 cm^{-1} is related to the defect complexes [57]. Kaschner et al. [55] suggested that the nitrogen concentration has a linear dependence with the 275 cm^{-1} peaks of Raman spectra.

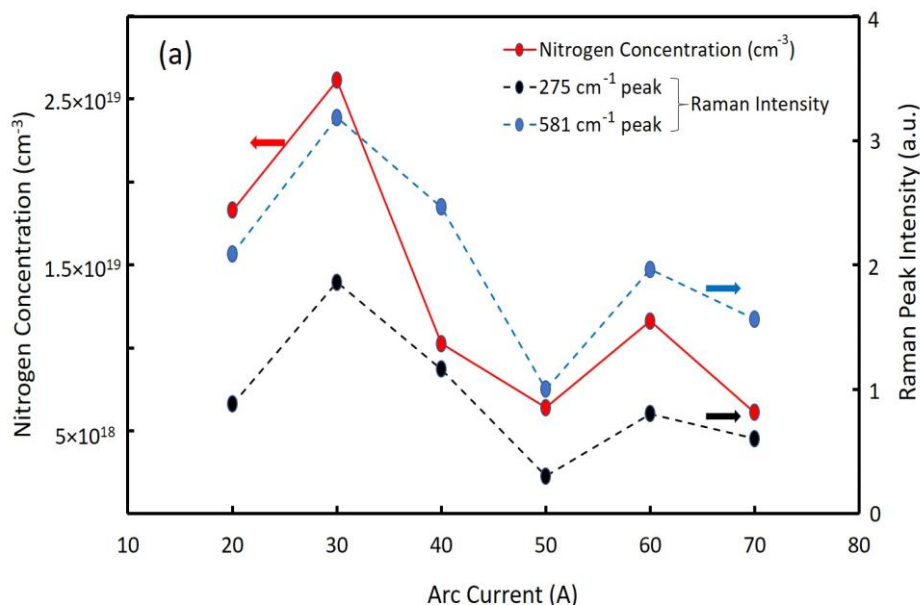


Figure 8. The Raman peak intensity (275 cm^{-1} and 582 cm^{-1}) (dot line) and nitrogen concentration (solid line) as a function with the arc current condition of 20 A ~ 70 A (Reference [49]).

2.2.3 X-ray diffraction

ZnO lattice belongs to crystal structures such as wurtzite, zinc blende, and rock salt. The wurtzite structure of ZnO consists of hexagonal symmetry. The hexagonal symmetry is characterized by constant lattice parameters of a and c . The lattice constants of ZnO depend on external stress impurities. The lattice crystal structure of ZnO NPs affected by the incorporation of impurities and studied the modified lattice properties through X-ray diffraction (XRD). A diffractometer (Smart Lab Rigaku Corporation) with $\text{CuK}\alpha$ radiation was used for measuring the XRD of the ZnO powder samples. **Figure 9** shows the illustration of the wurtzite crystal structure of ZnO.

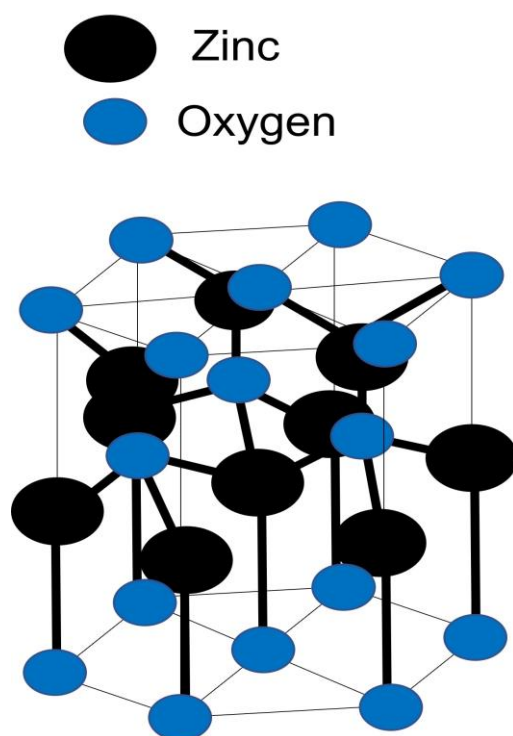


Figure 9. The hexagonal structure of ZnO with wurtzite crystal.

The structural morphologies of N-doped ZnO NPs were examined, which was followed at the chamber pressure of 150 T and the arc current of 30 A, by XRD measurement as expressed in **Figure 10**. The peak pattern of X-ray diffraction for the powder ZnO NPs samples can well describe the hexagonal wurtzite crystal structure with proper orientation and consistent with the standard JCPDS data (36-1451) [35] for ZnO. No additional peaks appeared due to other impurities. ZnO's wurtzite structure belongs to the space group C_{6v}^4 [58] and consists of the optical Raman-active phonon mode observed in the Raman spectra of ZnO NPs. The XRD diffraction peak (002) of N-doped ZnO NPs appeared at a 34.31° angle, which is shifted compared to the diffraction peak (002) for bulk ZnO (34.42°) [59]. The peak shift was appeared due to the difference of lattice constant by the high concentrate nitrogen in ZnO NPs lattice. The lattice constant of XRD of ZnO NPs was calculated. The lattice parameter a-value was 3.26 \AA and c-value was 5.22 \AA , which

was the variation of the ideal lattice constant for ZnO (3.24 Å, 5.20 Å). The results were evidence of the inclusion of nitrogen into the ZnO NP crystal lattice.

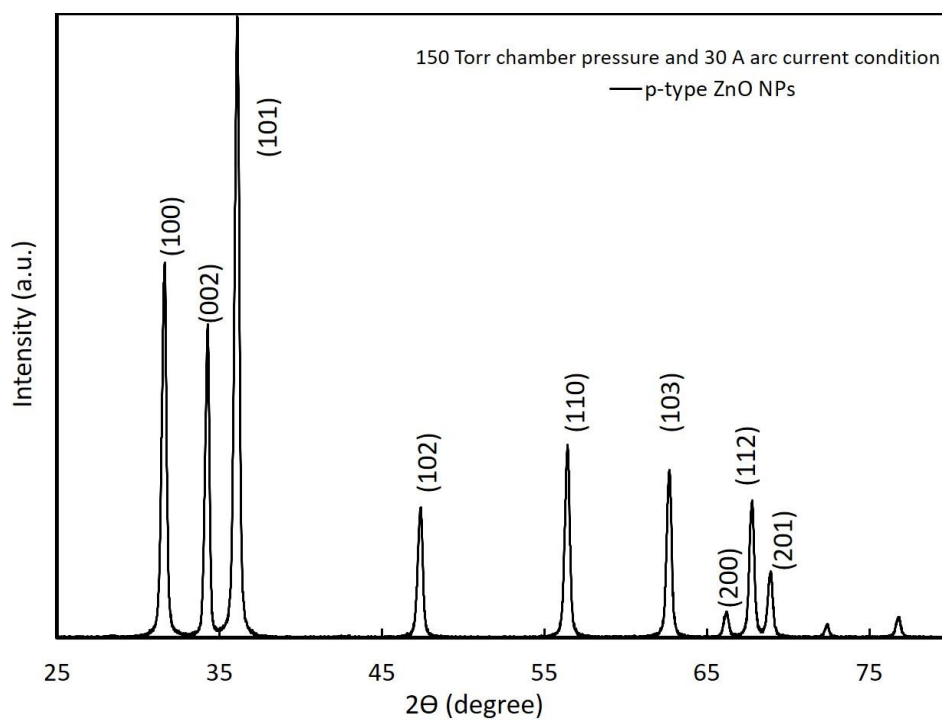


Figure 10. X-ray diffraction of N-doped p-type ZnO NPs (Reference [49]).

2.2.4 PL

To study the carrier recombination properties of the ZnO NPs, a Horiba FluoroMax-4 Spectrofluorometer with an excitation wavelength of 325 nm using a Xe lamp was used to detect the PL spectra at room temperature. **Figure 11** mentions the PL spectra at near band edge (NBE) emission and broad visible emission of the prepared ZnO NPs, which was generated at the chamber pressure of 150 Torr and the arc currents of 20 A to 70 A. The near band edge (NBE) and deep level emission peaks were observed from the PL spectrum. The deep level emission occurred due to the point defect related transition of ZnO NPs. Because ZnO has native or intrinsic defect phenomena like oxygen vacancies (V_o), zinc vacancies (V_{Zn}), and zinc interstitials (Zn_i), etc [60]–[62]. In the PL spectrum of as-prepared ZnO NPs samples, the defect-related deep level emission increased due to oxygen deficiency (V_o) by introducing the efficient acceptor nitrogen at oxygen sites in ZnO lattice. The NBE emission peak shifted toward the lower energy side because of the donor-acceptor pair (DAP) transition [63]. The NBE emission of ZnO NPs was found comparably strongest at the arc current of 30 A compared to other arc currents.

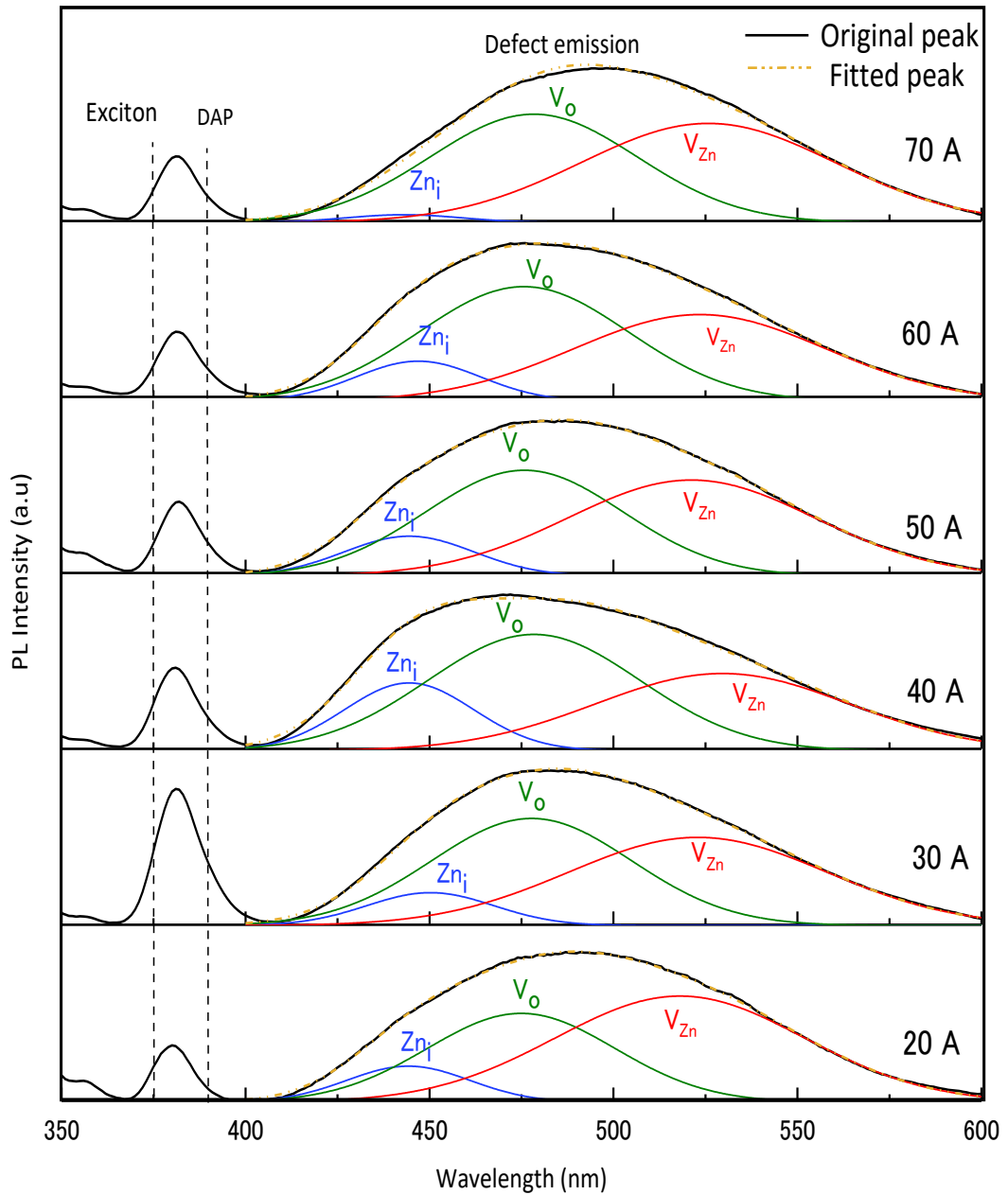


Figure 11. PL emission spectra of N-doped p-type ZnO NPs (The preparation condition of NPs was at the chamber pressure condition of 150 Torr and the arc current of 20 A to 70 A).

The acceptor nitrogen incorporation in the ZnO NPs crystals is revealed in their Gaussian deconvolution of PL spectra at near band edge (NBE) emission through the occurrence of donor-acceptor pair (DAP) recombination [64]–[66]. The intensity of DAP emission increased with the increasing nitrogen concentration in the ZnO NPs crystal, which is reflected in the acceptor levels of ZnO NPs. Zeuner et al. [67] suggested the nature of the DAP band at 3.24 eV for nitrogen-doped ZnO. **Figure 12 (a)** represents the NBE emission and the deconvolution peaks corresponding to the DAP and exciton emission. The observation was found that the DAP band emission was centred on a strong signal at about 3.23 eV, and the vigorous band intensity confirmed the involvement of nitrogen acceptor in ZnO lattice [68]. **Figure 12 (b)** shows the ratios DAP/exciton emission plot versus Raman peak 275 cm^{-1} intensity in the respective samples. The DAP and exciton emission intensity ratios were nearly proportional to the ZnO NP lattice's nitrogen content, revealing 275 cm^{-1} peak intensities of Raman spectra. In this case, the nitrogen concentration of the ZnO NPs crystal correlates with the acceptor concentration in the ZnO lattice. Thus, it can be assumed that incorporating nitrogen in the p-type ZnO NPs acts as an acceptor.

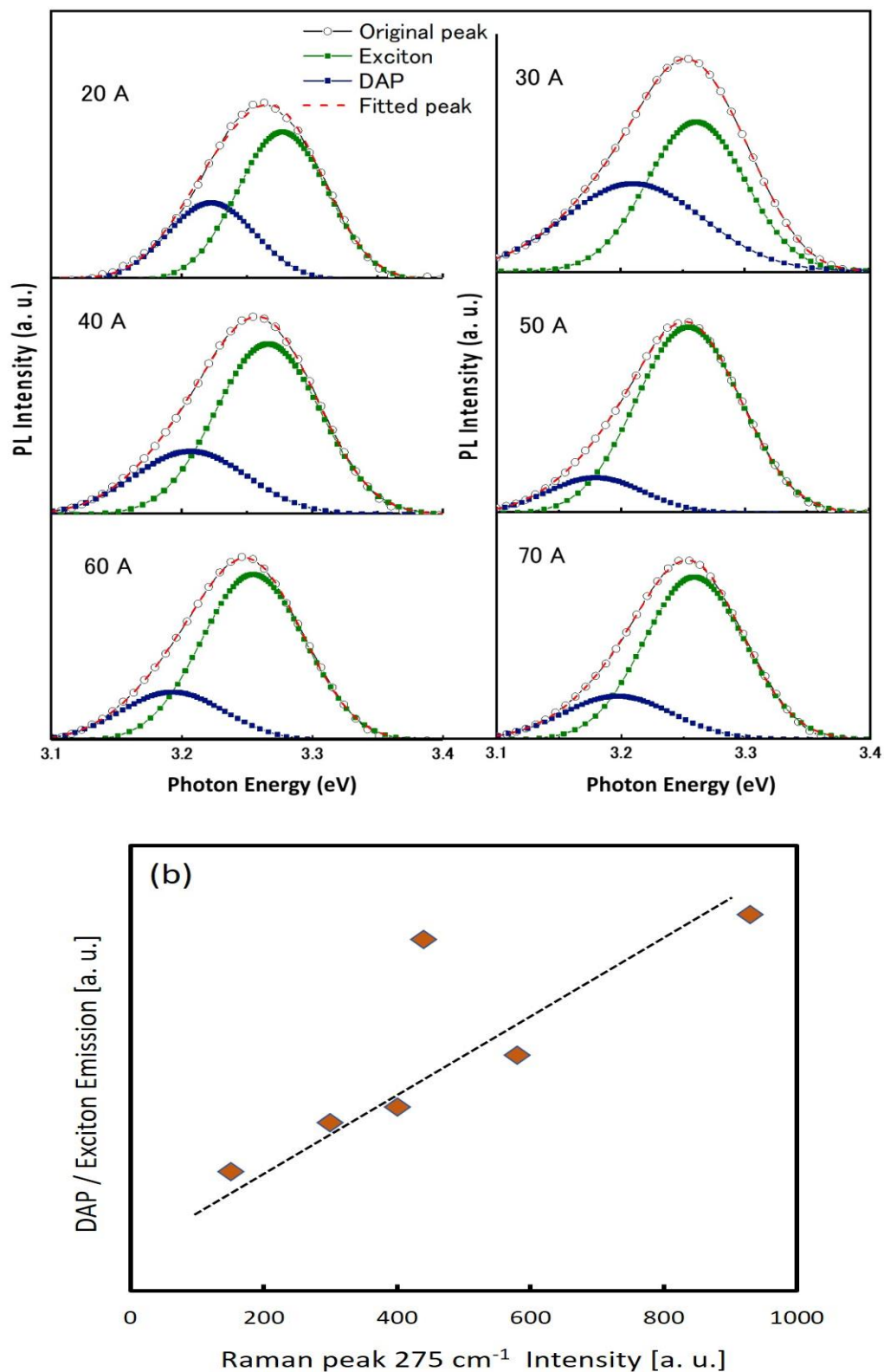


Figure 12. (a) is the Gaussian deconvolution for NBE emission of PL spectra of N-doped p-type ZnO NPs (Reference [49]) (b) is the ratios of DAP / Exciton emission versus Raman peak 275 cm⁻¹ intensity.

3. Fabrication and characterization of ZnO: N NPs (p)/ GZO UV LEDs

3.1 Fabrication of LEDs

For fabrication of LEDs, N-doped ZnO NPs used as a hole transporting p-type layer. The p-type ZnO NPs dispersion prepared by mixing with p-type ZnO NPs (0.05g), Isopropyl Alcohol (IPA) (0.3 ml), and binder (0.1g) (Silsesquioxane OX-SQ SI 20, Toagosei Co., Ltd) for the fabrication of LEDs. The ZnO NPs dispersion coated on the GZO electrode film (thickness of 500 nm) by a spin coating process. The GZO (Ga-doped ZnO) films were prepared using a 5% Ga-doped ZnO target on a 500 μm thickness of glass substrate by RF magnetron sputtering at the temperature of 300°C. The spin coating process followed two-step rotational conditions at the first speed of 1000 rpm for 5 sec and a final speed of 4000 rpm for 10 sec. A hot plate sintered the p-ZnO NPs coated layer at ~300°C. Gold (Au) electrodes with 30 nm thickness were deposited on both p-type layer and GZO film as a contact electrode using vacuum deposition procedure. **Figure 13** shows the schematic structural view of ZnO-based LEDs using a p-type layer on GZO electrode film. The contact electrode of Au shape on the p-type layer was 1 mm square and on the GZO film was the larger shape.

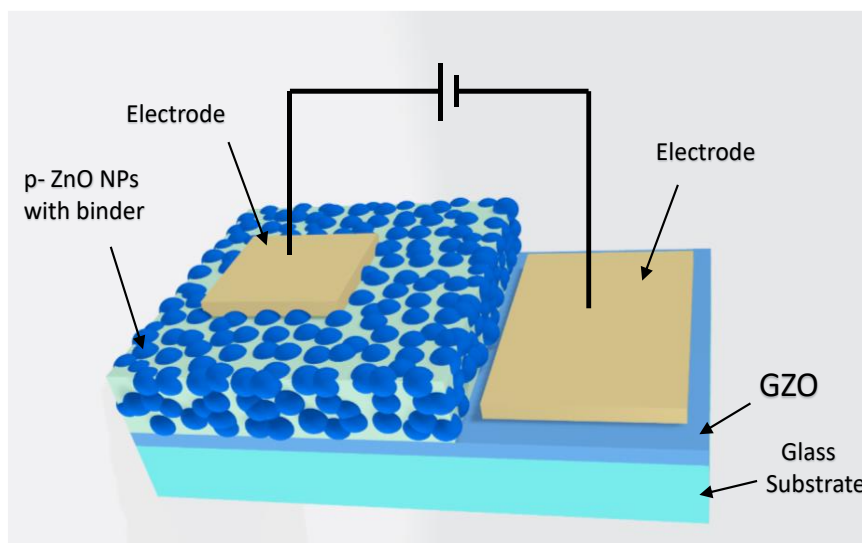


Figure 13. The schematic view of ZnO-based LEDs (Reference [48]).

3.2 *I-V* characterization

LEDs' current-voltage (*I-V*) measurement was performed using a parameter analyser (B2900A series of High-Resolution SMU module Keysight Technologies). We fabricated LEDs using N-doped p-type ZnO NPs. We chose to prepare N-doped ZnO NPs at the chamber pressure of 150 Torr and the arc currents between 20 A to 70 A. **Figure 14** displays the *I-V* properties of the fabricated ZnO NPs LEDs. The *I-V* characteristics of LEDs revealed a diode rectification character under dark conditions at room temperature. The device resistance under forwarding bias was noticed from the *I-V* curve due to the high resistivity of the ZnO NPs. The leakage current was observed from the devices, but the meaning of leak current variety for various conditions of ZnO NPs is still unknown and requires further investigations.

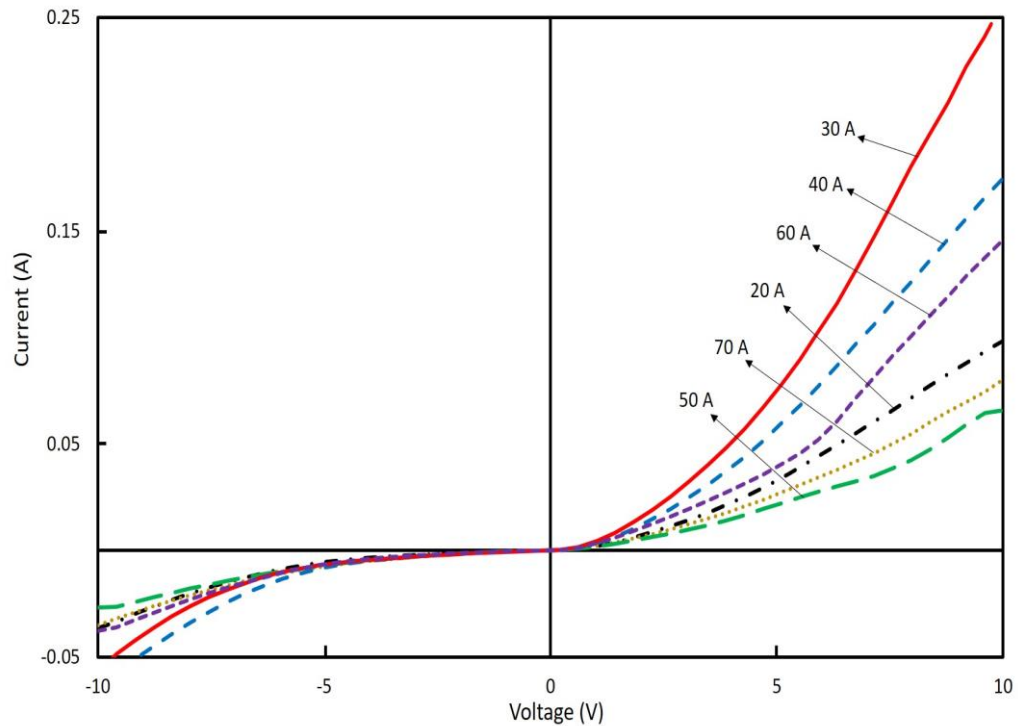
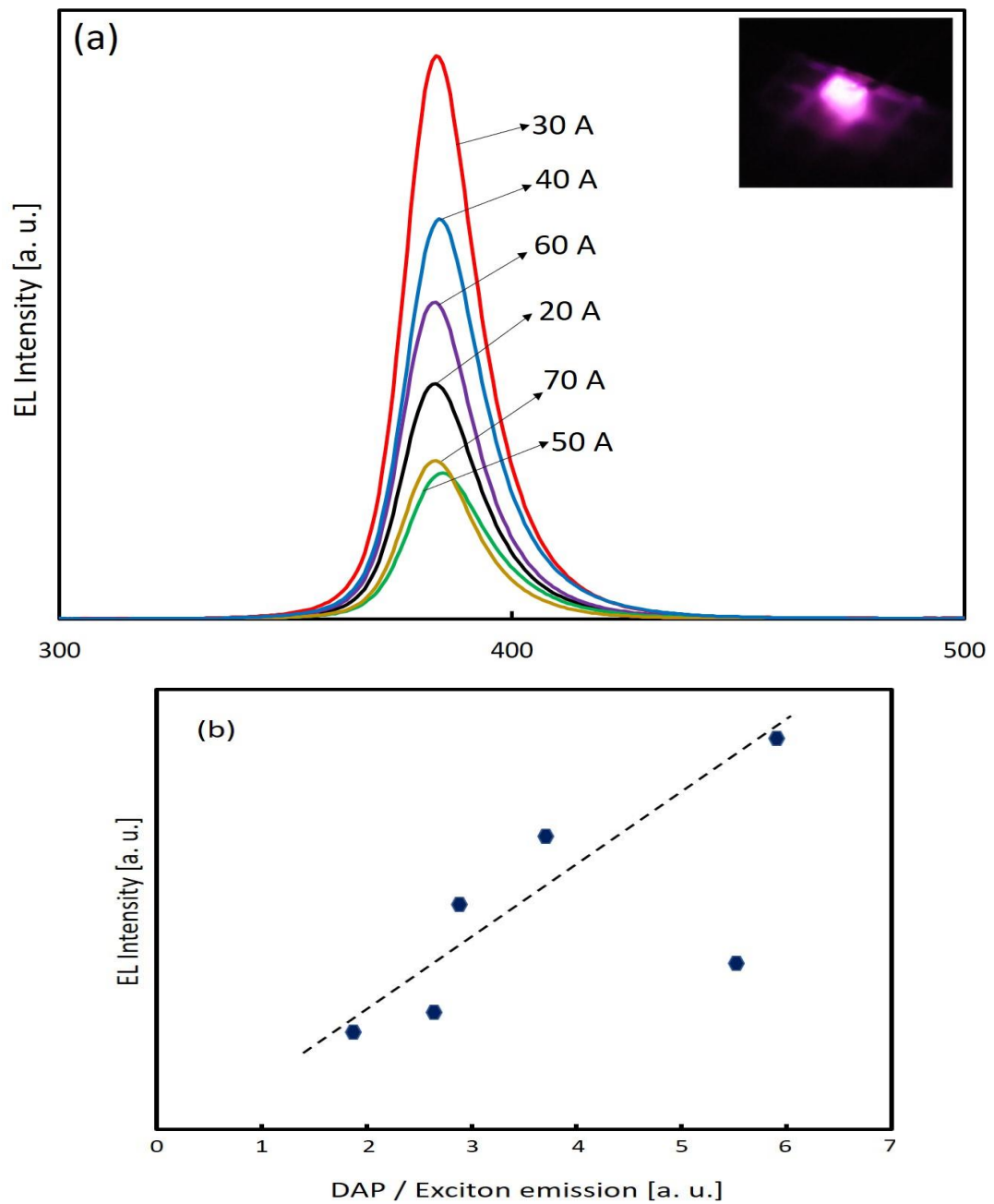


Figure 14. *I-V* characterization of ZnO NPs based LEDs (Reference [49]).

3.3 EL.

The EL was evaluated from the top side of the p-contact electrode at room temperature using the Ocean Optics QE65000 fiber multi-channel monochrome meter. The EL properties of ZnO NPs LEDs were measured at a forward bias voltage of 10 V, shown in **Figure 15** (a). The EL intensity of LEDs identified the near band edge UV emission. We did not observe the deep level emission in EL spectra, which were kept in PL spectra excited by a weak power source because the higher density excitation limited the deep level transition. **Figure 15** (b) expressed the EL intensity of LEDs versus the DAP/exciton emission of PL intensity of these p-type ZnO NPs. The device's EL intensity depends on the nitrogen content in p-type ZnO NPs, which is shown in the relation between nitrogen involved LVM of Raman peak (275 cm^{-1}) intensity and the EL intensity of the LEDs shown in **Figure 15** (c). Therefore, The EL emission intensity of the devices is near proportional

to the acceptor nitrogen concentration of the ZnO NPs crystal. Finally, we found that the electroluminescence properties of the devices were better at the chamber pressure condition of 150 Torr and the arc current of 30 A compared to other conditions that are in agreement with the higher nitrogen concentration of this conditional prepared ZnO NPs.



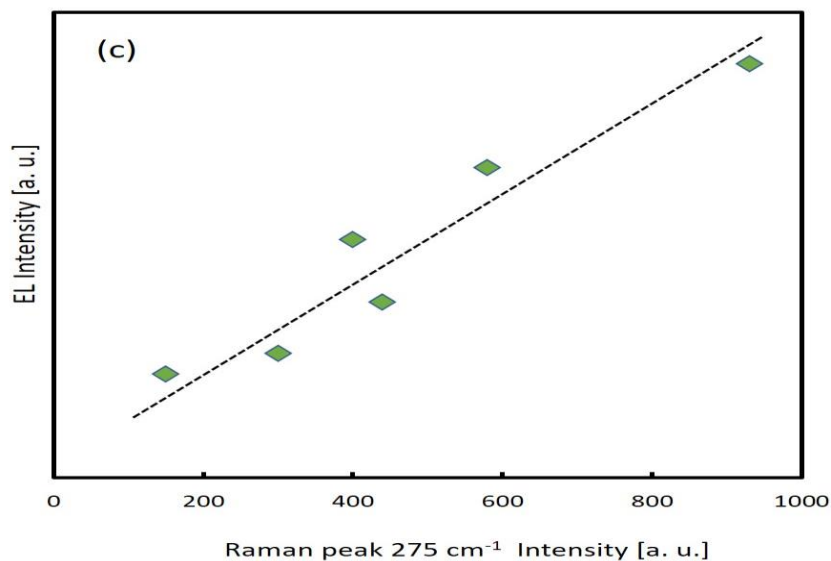


Figure 15. (a) The EL spectra of ZnO NPs LEDs (Inset shows the UV emission of LEDs) (Reference [49]) The graph of EL intensity of LEDs versus DAP/exciton emission (b) and Raman peak intensity of p-type ZnO NPs (c).

3.4 Conclusion:

The acceptor nitrogen dopants in ZnO NPs successfully carried out by DC arc plasma gas evaporation. The nitrogen concentration was measured by a thermal conductivity detector. The surface adsorbed species of N₂ molecules contained in ZnO NPs crystal. It was considered the Raman peak intensity of 275 cm⁻¹ as the nitrogen content in ZnO NPs. The PL of ZnO NPs was conducted to investigate the exciton and donor-acceptor pair (DAP) emission. The DAP/exciton emission ratios are near proportional to the Raman peak intensity of 275 cm⁻¹. The LEDs were fabricated using the N-doped ZnO NPs and observed the diode characteristics of the LEDs. The enhancement of the EL emission of the LEDs was near proportional to the ratios of DAP/exciton emission and the Raman peak of 275 cm⁻¹. The results indicated that the efficient nitrogen dopants in ZnO NPs acted as a suitable acceptor.

4. Fabrication and characterization of ZnO: N NPs(p)/ZnO: Ga NPs (n)/GZO homo-junction UV LEDs

4.1 Materials preparation

Shafiqul et al. [48] reported that the preparation of N-doped ZnO NPs with the radicals (oxygen and nitrogen) created in the air plasma using a zinc-metal vapor technique. In our group previously reported the detailed about the whole experiment process and mechanism of the NPs preparation [69]. In the experiment, zinc metal (Nilaco corporation - Zn 99.99%) ingot was prepared and placed inside the chamber as a zinc source. Dry air with a 5 L min^{-1} flow rate was entered in the chamber and played a role as the source of oxygen and nitrogen. An arc current induces a simple oxidation process at 20 A to 70 A between the cathode of carbon and the anode of metal zinc source. The pressure inside the chamber was controlled at 150 Torr and 610 Torr by the monitoring valve and the rotary pump throughout the preparation time of NPs. The chamber pressure at 150 Torr and arc current of 30 A were followed for preparing p-type conductivity ZnO NPs as a hole injection layer. The chamber pressure of 610 Torr and arc current of 70 A used to prepare ZnO NPs and doped with Ga for n-type conductivity as an electron transporting layer.

Intentionally n-type doping has been chosen using efficient donors like the group III-oxide (Ga_2O_3), which can easily substitute on the host ZnO site act as shallow donors in ZnO lattice. Ga-doped ZnO NPs are prepared by thermal diffusion of Ga into ZnO. In this case, the synthesized ZnO (610 Torr chamber pressure) NPs (0.1 g) and Ga_2O_3 (0.015 g) (Sigma Aldrich Co. Ltd.), which as a Ga source, were mixed and annealed in an electric furnace at $\sim 900^\circ\text{C}$ temperature under N_2 ambient flow (0.5 L min^{-1}) for 1 hour. In the furnace, the temperature increased from room temperature to 900°C within 10 min, and after 1-hour of thermal treatment, the Ga-doped ZnO NPs samples were cooled down to

less than 40 in 2 hours. In this research article explained the detailed of experimental procedure for the preparation of Ga-doped ZnO NPs [37]. **Figure 16** shows the preparation process of Ga-doped ZnO nanoparticles.

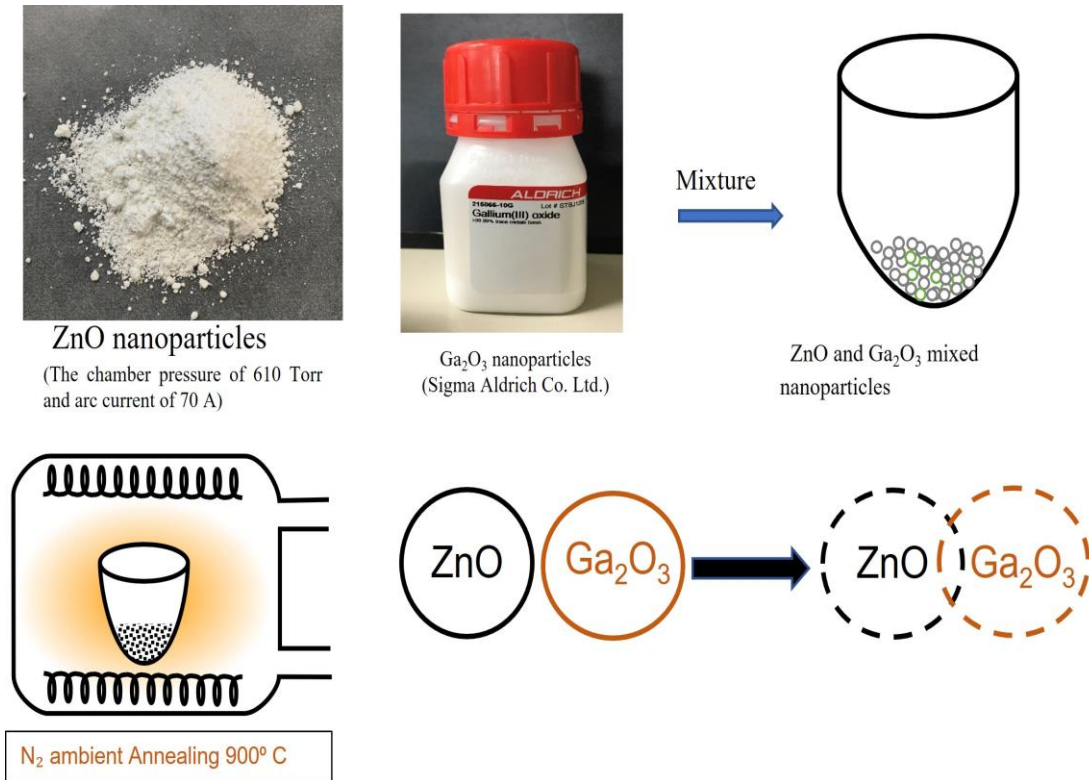


Figure 16. The preparation process of Ga-doped ZnO NPs using thermal ambient.

4.2 X-ray diffraction of as-prepared ZnO NPs and Ga-doped ZnO NPs

Shafiqul et al. [48] presented that the efficient donors for n-type doping were intentionally chosen, like the group III-oxide (Ga_2O_3), which can easily substitute host ZnO site acting shallow donors in ZnO. **Figure 17** expresses the X-ray diffraction (XRD) of the powder samples of as-prepared ZnO NPs, which was prepared the pressure of 610 Torr and arc current of 70 A, and Ga-doped ZnO NPs. The XRD peak of the synthesized ZnO NPs and Ga-doped ZnO NPs has narrated the structure of hexagonal wurtzite crystal with accurate orientation in agreement with the standard JCPDS data (card no. 36-1451) [35] for ZnO. Some excessive peaks were attributed in the XRD of Ga-doped ZnO NPs according to Ga_2O_3 NPs compounds after annealing with as-prepared ZnO NPs. Diffraction (002) peak (34.29°) for as-prepared ZnO NPs indicated the angular position toward lower side compared to that of bulk ZnO (34.42°) [70] because of the difference of the lattice constant due to nitrogen introduced in the ZnO NPs. In Figure 17, the inset of right side defines the 002 peak of XRD for as-prepared ZnO NPs and Ga-doped ZnO NPs. It exhibits that the observation of (002) peak position (34.326°) of Ga-doped ZnO NPs is a slightly toward the higher angle compared to the as-prepared ZnO NPs peak position (34.29°). The reason is the variation of lattice constant of the as-prepared ZnO NPs and the Ga-doped ZnO NPs. The lattice parameter of as-prepared ZnO NPs was 3.263 \AA for a-value and 5.225 \AA for c-value. On the other hand, the lattice parameter of as-prepared ZnO NPs was 3.260 \AA for a-value and 5.221 \AA for c-value. The degradation of lattice parameter of Ga-doped ZnO NPs was happened due to the contamination of foreign materials (Ga doping) in the host ZnO lattice. This is the actual consequence due to the size variety of ionic radius Zn (0.60 \AA) and Ga (0.47 \AA) [71]. The phenomenon is due to small size of the Ga atom deformed the ZnO lattice and decreased the lattice constant. H. Gomez et al. [71] reported that the

reduction of the lattice parameter (c) depended on the ratio of excess Ga content in the ZnO lattice.

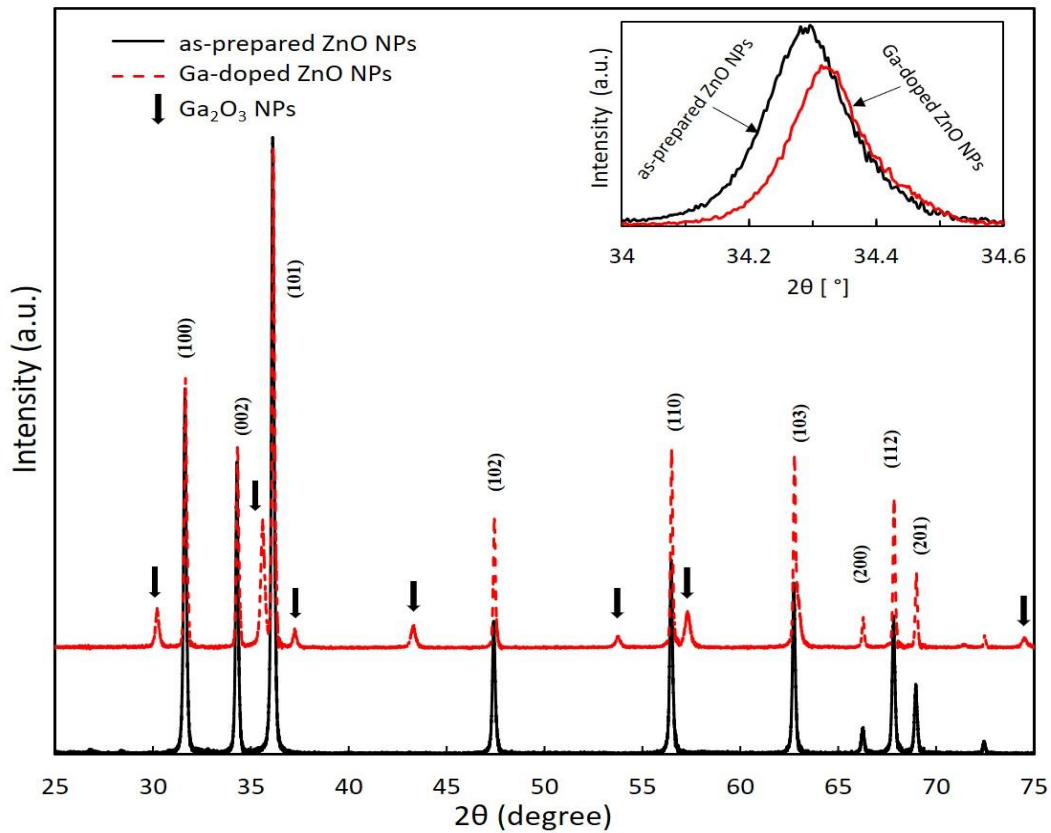


Figure 17. X-ray diffraction spectra of the as-prepared ZnO NPs and Ga-doped ZnO NPs. The inset shows a comparison of the diffraction peak (002) for the as-prepared ZnO NPs and Ga-doped ZnO NPs (Reference [48]).

4.3 PL Comparison

The PL measurements of as-prepared ZnO NPs, and Ga-doped ZnO NPs sprayed layer on the substrate were conducted. **Figure 18** shows the PL spectra of as-prepared ZnO NPs and Ga-doped ZnO NPs. A weak source of Xe- lamp was used to mark the defect emission by weak excitation conditions. A sharp UV emission was found at around 380 nm resembling to the near band edge (NBE) transition of ZnO [72]. A broad deep-level

emission was attributed to the point defect-related transition of ZnO NPs [73]. The broad emission was appeared due to the native defects like vacancies (V_{Zn} , V_O) and interstitials (Zn_i) [74]. The near band edge of PL intensity for Ga-doped ZnO NPs was improved, which was referred from the comparison of PL spectra results. Because the role of Ga atom as an activated donor led to raise the charge carriers. The Ga-doped ZnO NPs defect level emission showed a significant reduction when placed into the vacant site in ZnO. It can be supposed that the extrinsic dopant shallow donor Ga is dominant in the zinc site and composed of substitutional Ga atoms [18], [75]–[77]. The above discussion on PL spectra has indicated that the relatively lower defects of Ga-doped ZnO NPs was attained. These Ga-doped ZnO NPs can be possible to use for the application of n-type layer in the LEDs.

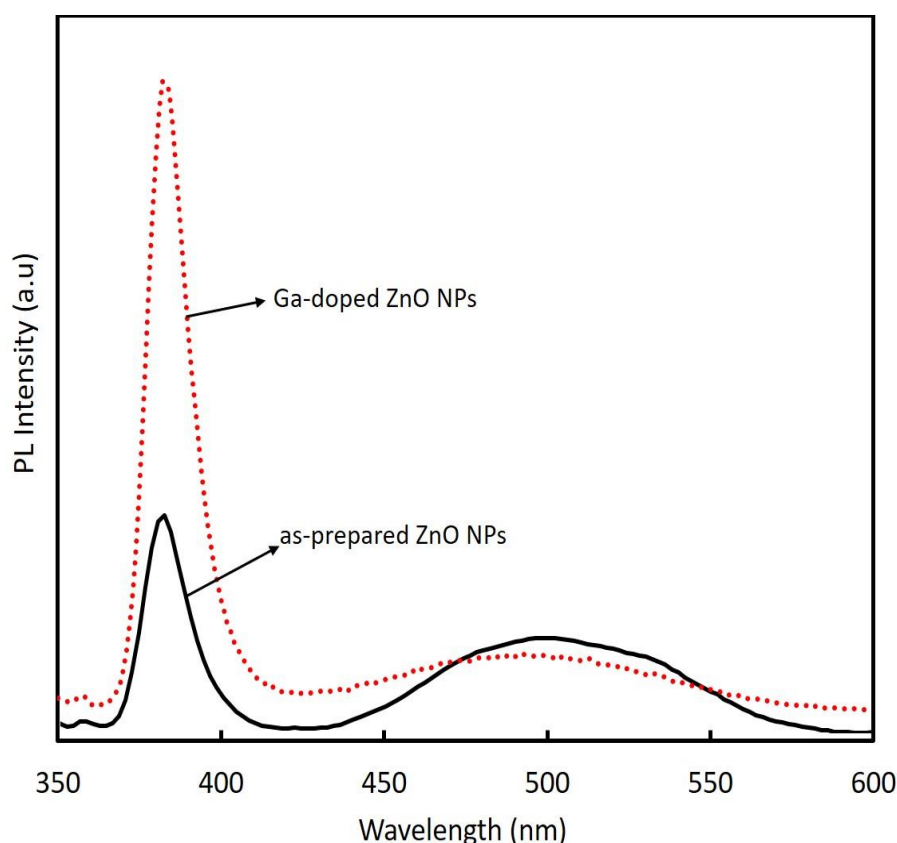


Figure 18. PL spectra of the as-prepared ZnO NPs (solid line) and Ga-doped ZnO NPs (dot line) sprayed layers.

Figure 19 shows the PL spectra of p-type ZnO NPs and Ga-doped n-type ZnO NPs. The comparison of PL spectra between N-doped ZnO and Ga-doped ZnO NPs indicates that the peak energy (3.246 eV) of NBE emission of PL spectra for the Ga-doped n-ZnO layer was shifted toward lower energy side compared with NBE peak energy (3.263 eV) for the p-ZnO layer as mentioned in Figure 19. The reason for the shift of lower energy side is possibly due to the enhancement of electron concentration and appearing donor-acceptor pair transition [78] in addition to the excitonic emission.

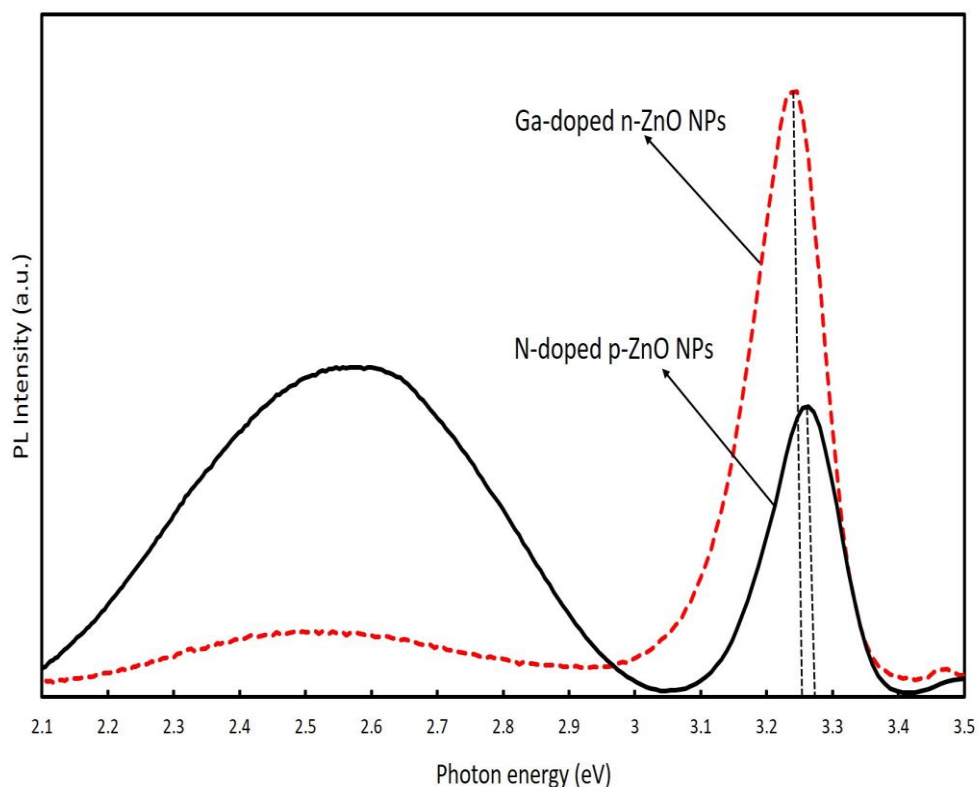


Figure 19. PL emission spectra for N-doped p-ZnO NPs (solid line) and Ga-doped n-ZnO NPs (dot line).

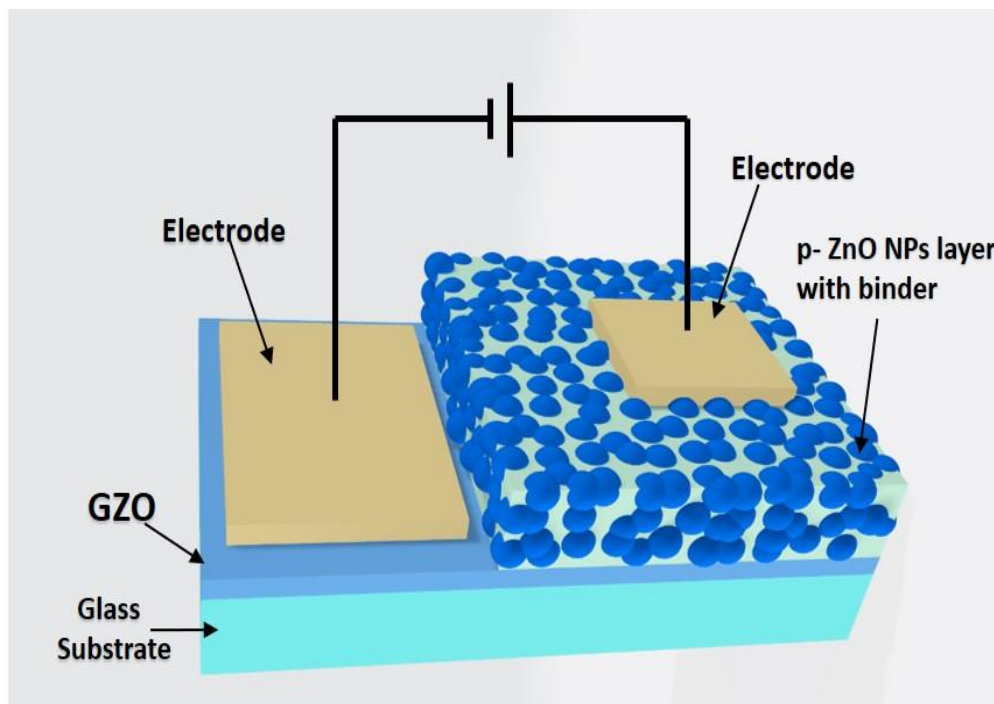
4.4 Hall measurement for ZnO nanoparticles

The electron mobility and carrier concentration of the ZnO NPs was conducted using the van der Pauw method (HL5500PC with HL5580 Buffer Amplifier, ACCENT). The Hall effect results are notable results that show the signs of carrier polarity. The mobility of N-doped ZnO NP film was approximately $4.61 \text{ cm}^2/\text{Vs.}$, and the Ga-doped ZnO NP film was about $6.63 \text{ cm}^2/\text{Vs.}$ The carrier concentration of N-doped ZnO NP films and Ga-doped ZnO NPs films were $3.2 \times 10^{13} \text{ cm}^{-3}$ for p-type conductivity and $-2.696 \times 10^{14} \text{ cm}^{-3}$ for n-type conductivity, respectively. However, these results dominate the property of grain boundaries (GBs) between NPs. Previous literature reported grain boundaries are contained in the nitrogen-doped ZnO layer [46], [79]–[81]. The carrier trap will be happened by the defect in GBs with creating the energy barriers. But this is dissimilar for the case of LEDs because the current flow of the LEDs in a direction of vertical to the NPs film surface and the number of boundaries is negligible.

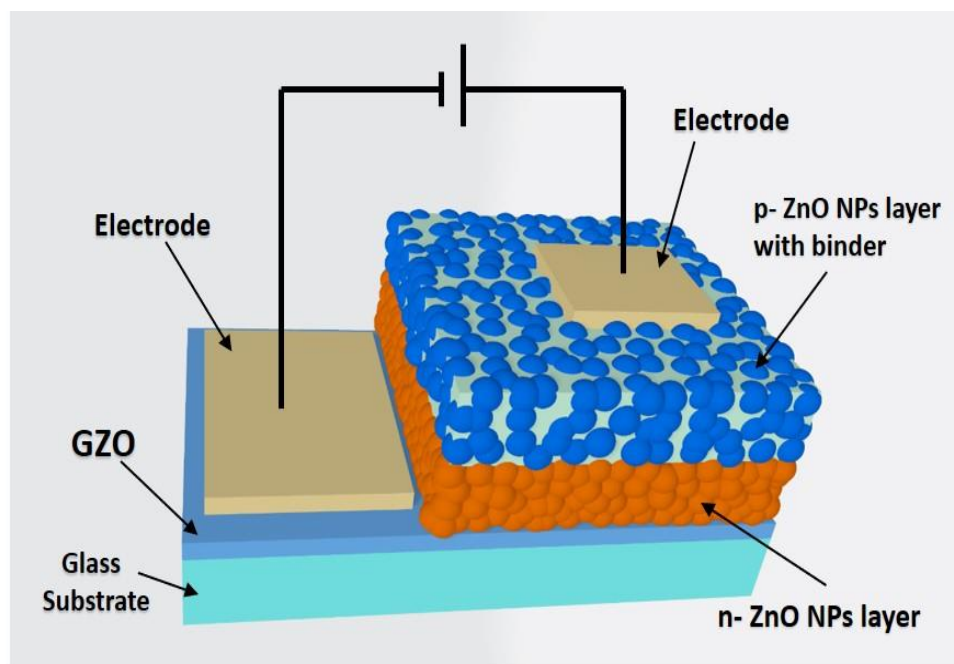
4.5 Fabrication of LEDs

According to Shafiqul et al. [48], two types of ZnO NPs LEDs were designed. A kind of LED had an N-doped p-ZnO NP layer placed on the GZO transparent electrode film. Another type had p-type layer of N-doped ZnO NP and n-type layer of Ga-doped ZnO NP coated on the GZO film as shown in **Figure 20** (a) and **Figure 20** (b), respectively. The GZO film (thickness of 500 nm) was prepared by the deposition of RF magnetron sputtering at 300 °C using a 5% Ga doped ZnO target on the thickness of 500 μ m white glass substrates. The dispersion of n- ZnO NPs were prepared using an ultrasonic homogenizer by mixing 20 g pure water with 0.2 g Ga-doped ZnO NPs. A centrifugal separator separated the large particles from the dispersion (3000 rpm, 1min). To form the n-ZnO NP layer, the divided dispersion was sprayed using an airbrush onto the GZO electrode film, which was on the hot plate at ~300 °C temperature.

The synthesized p-type ZnO NPs (0.05 g) was mixed with Isopropyl Alcohol (IPA) (0.3 ml) and (0.1 g) binder (Silsesquioxane OX-SQ ME 20, Toagosei Co., Ltd) to prepare p-ZnO NP dispersion. This dispersion was coated on the GZO and n-ZnO NP layer to fabricate LEDs. The spin coating process was carried out at an initial speed of 1000 rpm for 5 sec and accelerated to 4000 rpm for 10 sec. The coated NP layer was sintered on the hot plate at ~300 °C for 1 min. Finally, gold (Au) as a contact electrode with 30 nm thickness was deposited on both the p-ZnO NP layer (1 mm square) and transparent GZO film (large shape) using the deposition process.



(a)



(b)

Figure 20. Schematic view of ZnO NPs based LEDs. (a) p-ZnO NPs/GZO structure (b) p-ZnO NPs/n-ZnO NPs/GZO structure (Reference [48]).

4.6 SEM measurement

The ZnO NPs dispersion was prepared and measured the nanoparticles size of the ZnO. Using the ZnO NPs dispersion, the NPs layers were made and measured the SEM image of the ZnO NPs layers. A scanning electron microscope (SEM) (JEOL Ltd., JCM- 7000) was used to study the surface and cross-section image of the ZnO NP layer. A Horiba LB-550 dynamic light-scattering analyser was used for measuring the particles size of ZnO NPs dispersion. **Figures 21** (a) and (b) show the surface SEM image of the top layer of the ZnO NPs and the particles' size of the ZnO NPs dispersion, respectively. **Figures 21** (c) and (d) indicate a cross-sectional view of the LEDs with different structures. The p-ZnO NP layer on the GZO electrode and the p-ZnO NP layer and n-ZnO NP layer on GZO, respectively. We cut the samples with a diamond wire cutter to view the cross-section of the device layers. The samples were not cut precisely due to the NP layer during the cutting process. But it could be estimated that the thickness of the spin-coating p-ZnO NP layer was around 3 μm , and sprayed n-ZnO NP layer was about 2 μm thickness.

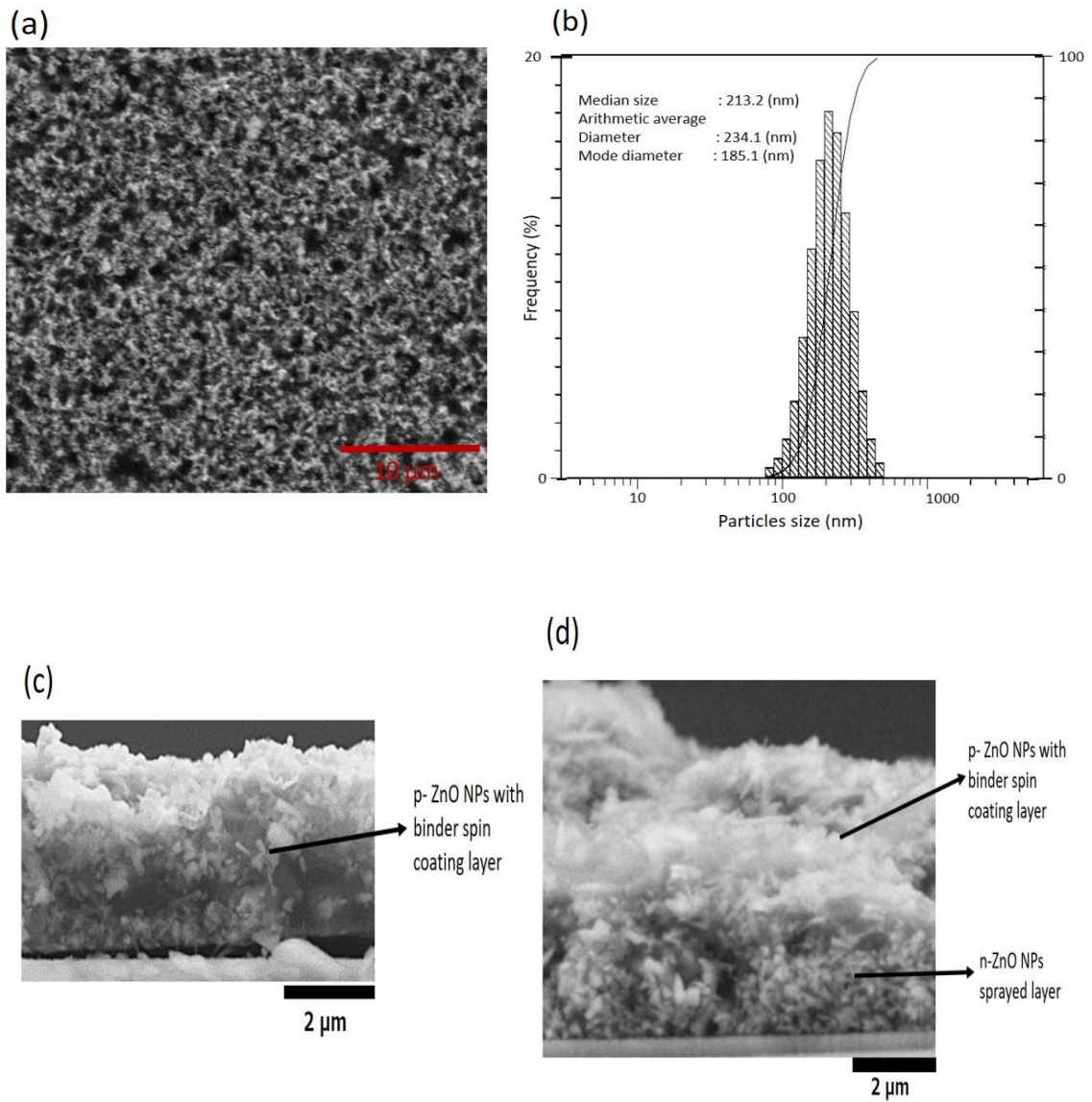


Figure 21. SEM surface image of the ZnO NP layers (a); particles size of the ZnO NPs (b); SEM cross section images p-ZnO NP layer (c), p-ZnO NP layer and n-ZnO NP layer (d) (Reference [48]).

4.7 *I-V* characteristics and light output power measurement

Shafiqul et al. [48] presented that the characterization of *I-V* and the intensity of EL power for the LEDs were measured. The electrical and optical properties of the LEDs were investigated under dark conditions at room temperature, as shown in **Figure 22**. The measurement of *I-V* curves with diode characteristics, and the emission of EL power were attained, where the turn-on voltage was around 3 V. That is mainly similar to the bandgap energy of ZnO. It was found from the *I-V* curve of the LEDs with a high resistance under forwarding bias condition due to the higher resistivity of the ZnO NP layers. The leakage current was observed [82]. The possible reason that the N-doped ZnO NPs for the p-type layer also consisted of n-type ZnO NPs because the arc plasma is unstable for synthesis. From Figure 22, the leakage current of the p-ZnO/n-ZnO/GZO LED structure was significant compared to that of the design of p-ZnO/GZO LED. This is perhaps that the roughness of NP layers was increased because the NP layer was inserted by a sprayed coating process. The EL power emission of the LEDs was carried out through the glass substrate onto the photodiode. The following equation used to evaluate the EL power calculation:

$$\text{The external efficiency, } \eta_c = 2\Omega_c / 4\pi \quad (1)$$

Here, $\Omega_c = 2\pi (1 - \cos \theta_c)$; critical angle, $\theta_c = \sin^{-1}(1/n)$.

The total EL power of the LEDs was calculated approximately 12 times larger than the observed value, only the glass substrate assumed an accurate reflection of the surface. The EL power for p-ZnO/n-ZnO/GZO LED indicates the droop effect in a high voltage region. This was mainly due to the higher current density of p-ZnO layer. The current pass through the p-type layer was compressed by the insulating binder and originated heat into the

device. The EL power for p-ZnO/n-ZnO/GZO LED is almost twice as larger as the p-ZnO / GZO LED at the voltage below the drooping area.

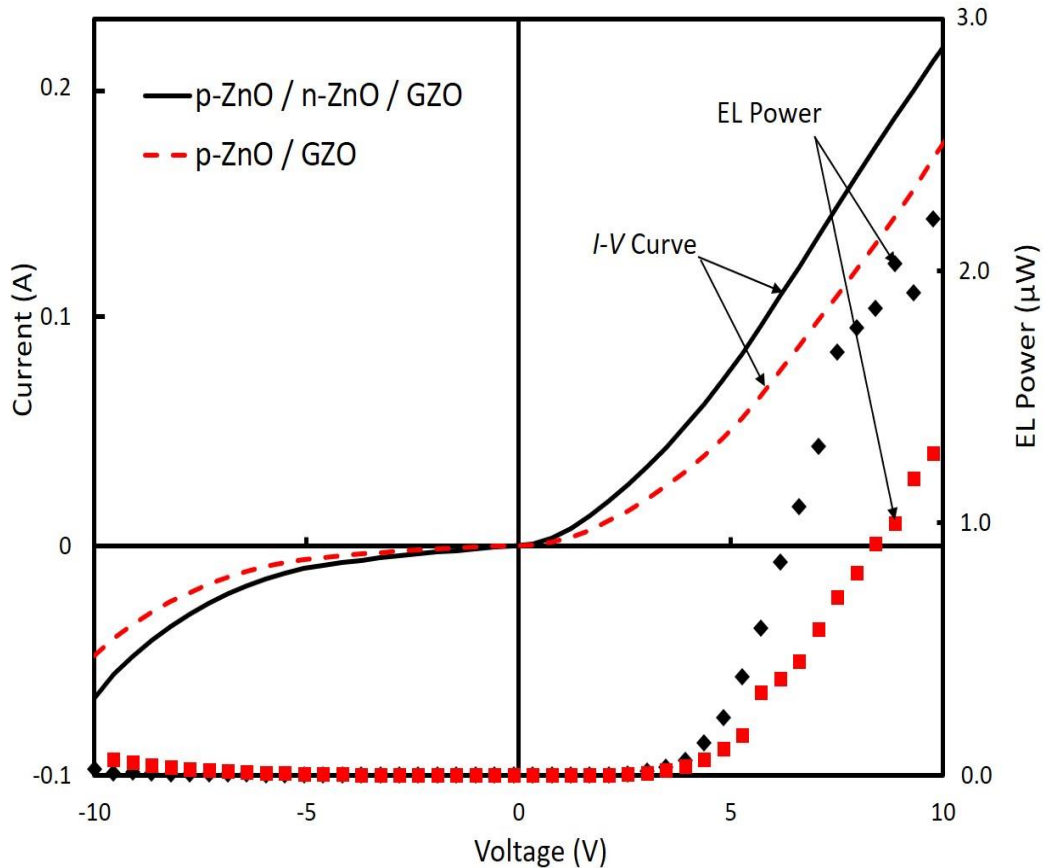


Figure 22. *I-V* characterization and EL power of ZnO NPs based LEDs with the structure of p-ZnO/n-ZnO/GZO and p-ZnO/GZO (Reference [48]).

4.8 EL

According to Shafiqul et al. [48] report, **Figure 23** shows the comparison of EL spectra for two different ZnO NPs based LEDs. The intensity of EL spectrum was increased particularly by adding the n- ZnO NPs active layer rather than without the n-ZnO NP layer. GZO electrode layers had not luminescence in these LEDs because GZO electrode film as a n-type layer has a very high carrier concentration (around $\sim 10^{21} \text{ cm}^{-3}$), where the weak luminescence n-GZO electrode layer acted as a current spreading layer to enhance the

uniformity of electron injection. In the formation of p-ZnO/GZO LEDs, electron injection had led GZO layer to carrier recombination in the p-ZnO NP layer because the active area exists only at this layer. On the other hand, the structure of p-ZnO/n-ZnO/GZO LEDs, n-type ZnO NP layer had low carrier density than GZO. The charge recombination would be generated in the n-ZnO NP layer, which acted as an active region. Thus, the magnification of EL was due to the addition of the n-type layer, and this layer was acting as a light-emitting layer. In that case, holes injection should be injected from the p-ZnO layer to the n-ZnO layer.

The EL emission peak energy for p-ZnO/GZO LED was found at around 3.20 eV, and the EL peak energy for the device added an n-ZnO layer (p-ZnO/n-ZnO/GZO) was observed near 3.23 eV, as shown in Figure 23. Both, EL peak energies for both LEDs were shifted toward the lower energy side compared to PL spectra. On the other hand, the EL peak of p-ZnO/n-ZnO/GZO showed higher energy than p-ZnO/GZO, which is the opposite of the PL result. It is one of the reasons that the energy shift of the EL toward the lower energy side due to the temperature rising and occurred the degradation of the bandgap energy [83]. If this is the actual purpose, a significant change should be happened in p-ZnO/n-ZnO/GZO LED because it had noticed a droop effect in the EL emission power, but the result is irrelevant. Another probable cause is red-shifts of EL that the carrier density of the higher injection by exciton-exciton collision and electron-hole plasma was occurred in the device, which was seen in the PL spectra at higher excitation densities [84], [85]. Taking this effect into account, it is consistent with the experimental result because the carrier flow passes at the p-ZnO layer with insulating binder will be concentrated. Resulting in, this p-ZnO NPs is comprise higher excitation density and the emission of EL is large redshift, but that in the n-ZnO layer will expanse to the NP layer without binder, as a result, the layer consists of lower excitation density and the emission of EL is smaller redshift.

The temperature of the structure (p-ZnO/n-ZnO/GZO) LEDs and the structure (p-ZnO/GZO) was calculated using the varshni model [83]:

$$E_g(T) = E_g(T=0) - \alpha T^2 / (T + \beta) \quad (2)$$

Where the temperature coefficients are, $\alpha = -5.5 \times 10^{-4} \text{ eVK}^{-1}$ and $\beta = -900 \text{ K}$ for temperature up to 300 K [86], [87]. The peak energy (3.23 eV) of EL spectra for the structure p-ZnO/n-ZnO/GZO LEDs calculated temperature was approximately 426 K. On the other hand, the peak energy (3.20 eV) of EL spectra for the structure p-ZnO/GZO LEDs temperature was approximately 450 K.

The EL emission of p-ZnO/n-ZnO/GZO LEDs was observed at 40 mA and 200 mA injection current. The peak position of EL at the low injected current of 40 mA was 3.243 eV, nearly the same as the PL peak energy (3.246 eV) of the Ga-doped n-ZnO NPs layer. On the other hand, the EL peak position of p-ZnO/n-ZnO/GZO LEDs at the high injected current of 200 mA was 3.23 eV, shown in **Figure 24**. The redshift of the EL was appeared due to the D-A pair emission that is also consistent with the results. The defect emission of the PL spectra was revealed which was excited by weak light source, which were not observed in EL spectra. Because the intensities of these emissions will saturate at such a strong excitation condition as these transitions are limited by the density of the levels, unlike excitonic emission. Thus, it can be considered that the evaluated EL emission of the structure (p-ZnO/n-ZnO/GZO) LEDs was ascribed owing to the radiative recombination was emerged in the n-ZnO NP layer as well p-ZnO layer.

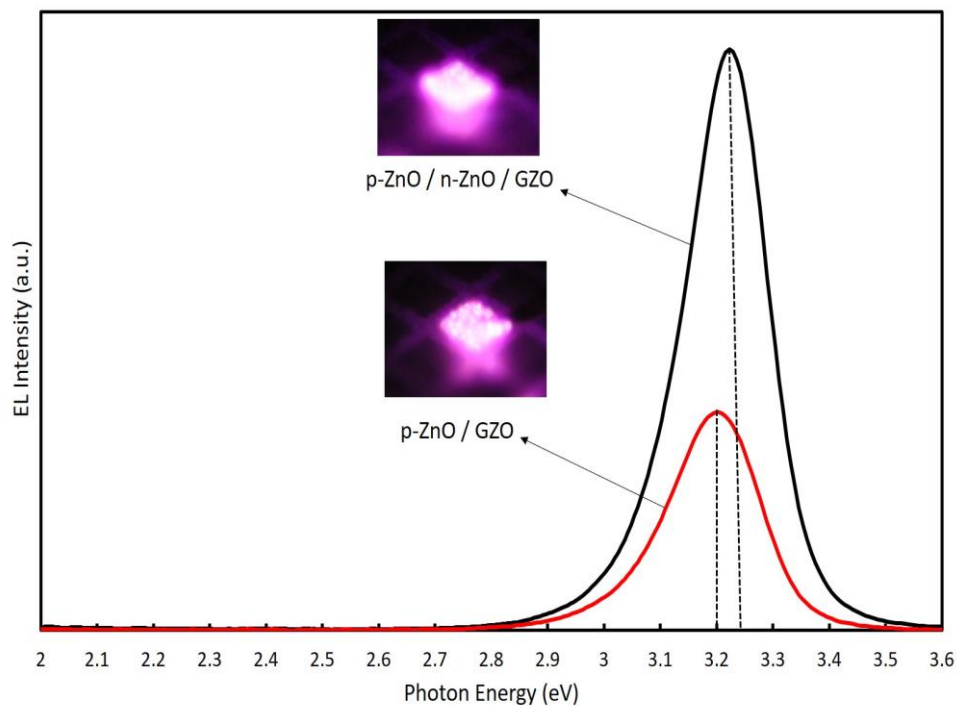


Figure 23. Comparison of EL spectra for ZnO NPs LEDs with the structure of p-ZnO/n-ZnO/GZO and p-ZnO/GZO. The LED's UV emission photographs show in the insets with the forward bias of 10 V (Reference [48]).

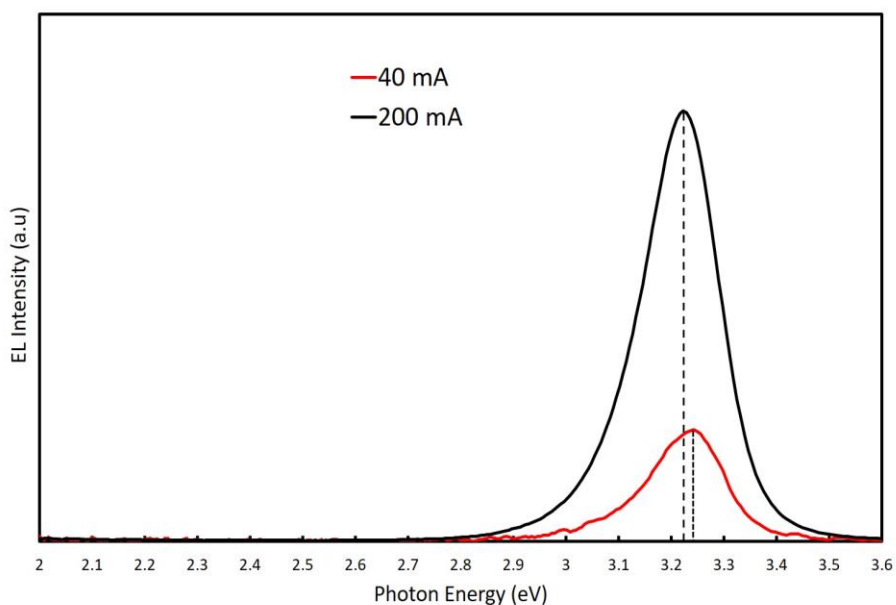


Figure 24. Comparison of EL spectra for ZnO NPs LEDs with the structure of p-ZnO/n-ZnO/GZO at the injection currents of 40 mA and 200 mA (Reference [48]).

4.9 Conclusion:

N-doped ZnO NPs and Ga-doped ZnO NPs prepared as p-type and n-type conductivity, respectively. The p-type and n-type ZnO NPs used to fabricate LEDs with the structure of p-ZnO/GZO and p-ZnO/n-ZnO/GZO. The evaluation of the characterization of the LEDs confirmed that the mechanism of LEDs showed as the p-n homo-junction devices, which is the world's first all nanoparticles-based LEDs. The EL power of the structure (p-ZnO/n-ZnO/GZO) LEDs enhanced doubled by inserting n-ZnO NPs layer compared to the structure (p-ZnO/GZO) LEDs.

5. The hetero-structure LEDs based on ZnO NPs by inserting ZnMgO NPs layer.

It was realized to improve the performance of optoelectronics and electronics devices by creating barrier layers and quantum wells in the hetero structure of the semiconductor devices. Because carrier confinement is an essential requirement for improving luminescence [88]–[90], carrier confinement can lead to high radiative recombination in the active region of the devices. Bandgap engineering is a necessary process for changing the energy structure of ZnO. The energy structure of ZnO has been changed by doping, surface modification, and size control [91]–[93]. The following equation determines the energy bandgap turning in a wide range.

$$E_g(x) = (1-x) E_{\text{ZnO}} + x E_{\text{AO}} - b x (1-x) \quad (3)$$

Where b is the bowing parameter and E_{AO} , and E_{ZnO} is the bandgap energies of the compounds AO (MgO) and ZnO, respectively.

MgO composite with ZnO can be an effective process for bandgap engineering by changing the conduction band and valence band [94], [95]. A considerable report presented one of the suitable candidates of ZnMgO alloy considered for the barrier layers by ZnMgO super-lattice structures. The ZnMgO alloy enables widening the bandgap energy of ZnO between 3.3 to 7.7 eV. The MgO exciton binding energy (80 meV) is larger than the wurtzite structure of ZnO (60meV). It can be advantageous to bode properly with Mg content for deep UV devices applications.

5.1 ZnMgO composite NPs preparation

We prepared ZnO NPs using the gas vapor technique with a chamber pressure of 610 Torr and an arc current of 50 A. The mechanism of the particles process is explained before the NP preparation section (2.1). The samples fabricated at the high pressure of 610 torr exhibit n-type conductivity [46]. For the preparation of ZnMgO composite NPs, the as-prepared ZnO NPs (0.1g) and MgO NPs (0.05g) were mixed with the vortex mixer. The ZnO NPs and MgO NPs mixture was placed in an electric furnace and annealed under an N_2 gas flow of 0.5 Lmin^{-1} inside the furnace. The furnace temperature was increased from room temperature to 1000°C within 10 minutes and kept constant for 60 minutes. The NPs samples were cooled down to less than 40°C in 2 hours. **Figure 25** shows the preparation process of ZnMgO composite NPs using a thermal treatment.

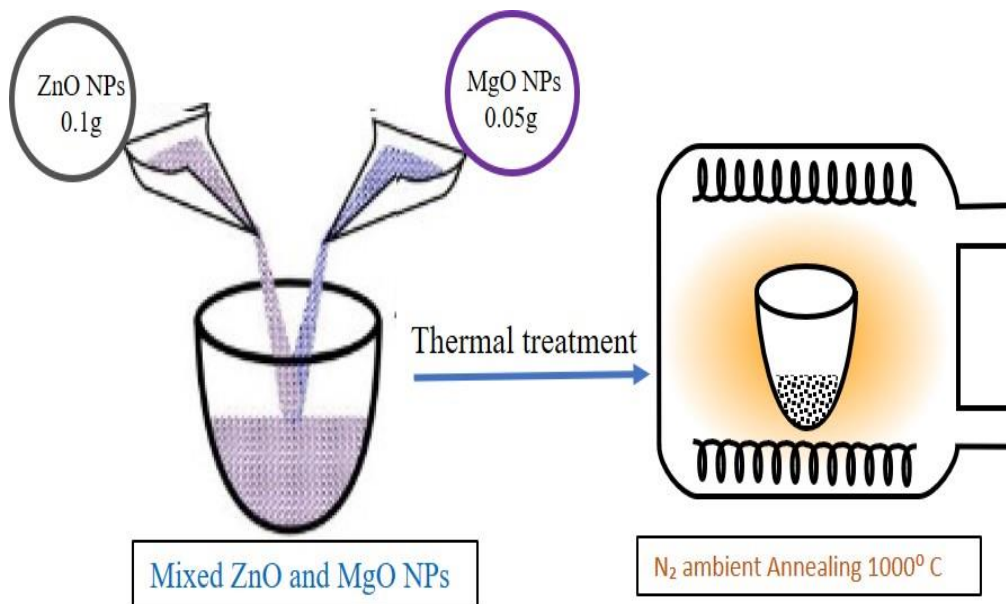


Figure 25. The preparation process of ZnMgO composite NPs using thermal treatment.

5.2 X-ray diffraction

Figure 26 shows the X-ray diffraction (XRD) patterns of the ZnMgO NPs and as-prepared ZnO NPs powder samples. The diffraction peaks of ZnO NPs and ZnMgO NPs had the hexagonal wurtzite structure, which agrees with ZnO's standard JCPDS (card no. 36-1451). The additional peaks attributed corresponding to the formation of MgO (No-7-239) [96] compounds from the presence of remaining MgO NPs after annealing. The shift of XRD peaks of ZnMgO NPs occurred toward the lower angle. The lattice constant of ZnMgO NPs was varied from the as-prepared ZnO NPs due to the inclusion of the foreign impurity (Mg^{+2}) imposed in the host ZnO lattice. This attribution happened due to the difference of ionic radius, where Mg ionic radius is 0.57 Å, and Zn is 0.60 Å [96]–[98]. The lattice constant of as-prepared ZnO NPs was 3.259 Å for a-value and 5.2207 Å for c-value. On the other hand, the lattice constant of ZnMgO NPs was 3.270 Å for a-value and 5.2361 Å for c-value. The ratios of the c/a lattice parameter were 1.6019 for as-prepared ZnO NPs and 1.6012 for ZnMgO NPs. The ratio of the c/a lattice parameter was decreased and affected the semiconductor bandgap, which consisted of the previously reported literature [99]. Vegard's law is a rule that expresses a proportional relationship between the lattice constant of the alloy and the concentration of composite elements [100]; for the composite $Zn_{1-x}Mg_xO$ NPs, the equation is-

$$A_{ZnMgO} = x A_{MgO} + (1-x) A_{ZnO} \quad (4)$$

where A is the lattice constant. From the experimental results, the lattice constant of as-prepared ZnO NPs is 3.259 Å, and that of ZnMgO is 3.270 Å. The lattice constant of MgO is 3.32 Å [101],[102]. It was calculated that the content (x) of Mg in the composite $Zn_{0.82}Mg_{0.18}O$ NPs was 0.18.

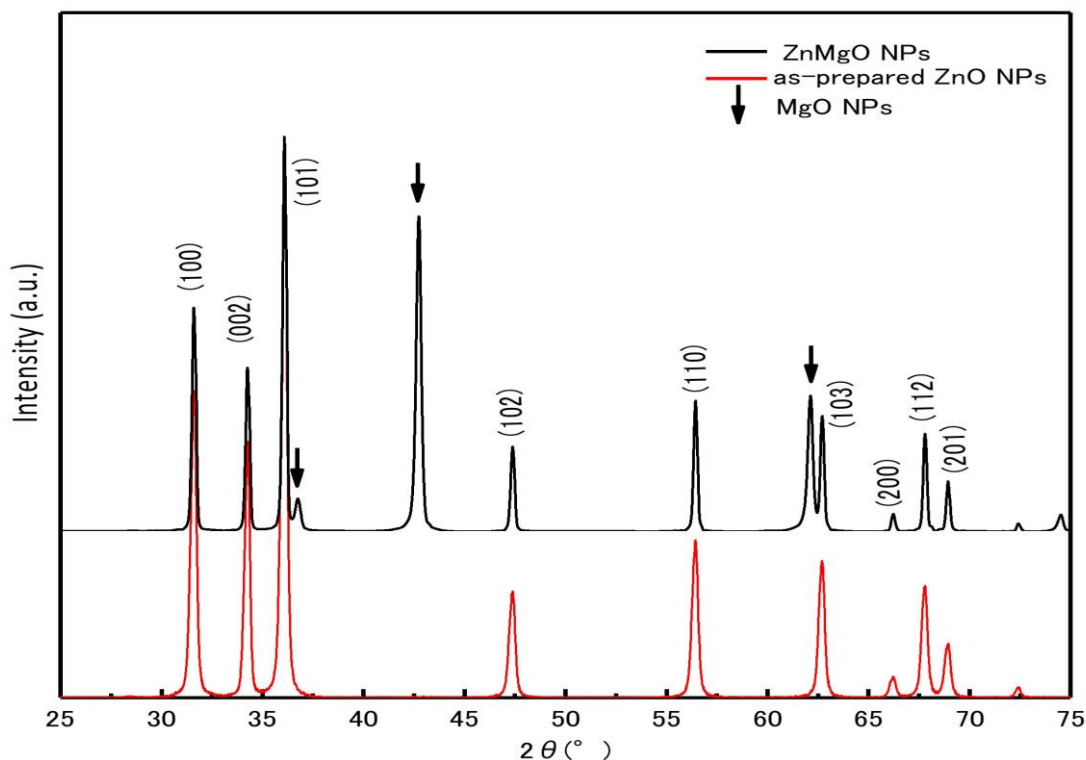


Figure 26. X-ray diffraction of as-prepared ZnO NPs and ZnMgO composite NPs.

5.3 Optical absorption

The optical absorbance spectra for as-prepared ZnO NPs and ZnMgO NPs at room temperature are shown in **Figure 27**. The peak energy of the absorbance spectrum for as-prepared ZnO NPs was exhibited at about 3.263 eV. On the other hand, a broad absorption with the peak energy position at about 3.376 eV was observed for the ZnMgO composite NPs. The peak energy of ZnMgO NPs shifted toward the higher energy side, which can be appeared due to the variation of bandgap energy [88], [103], [104].

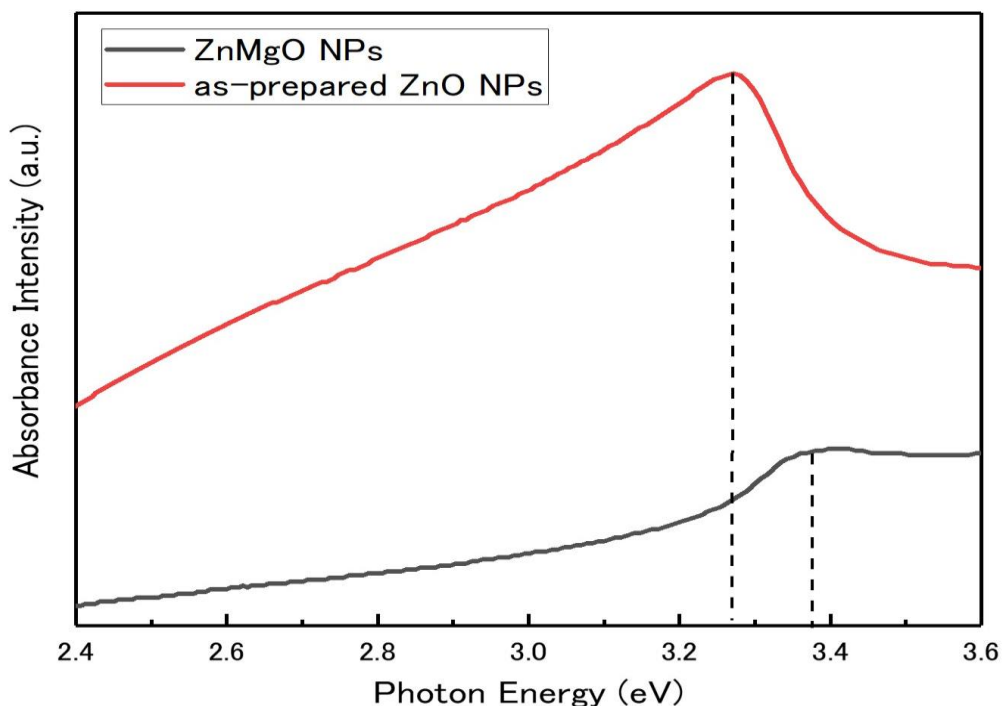


Figure 27. The absorbance of as-prepared ZnO NPs and ZnMgO composite NPs.

5.4 PL

Figure 28 shows the comparison of the results of the PL spectra for the as-prepared ZnO NPs and ZnMgO composite NPs. The observed peak position of the band edge luminescence for ZnMgO NPs was at about 3.278 eV and for the as-prepared ZnO NPs was at around 3.246 eV. The energy peak position of the ZnMgO NPs shifted toward a higher energy level than the peak energy of as-prepared ZnO NPs, which is consistent with the results of absorbance measurements. The difference of PL peak energy between the ZnO NPs and ZnMgO NPs is 32 meV. As we know, the bandgap energy of ZnO is 3.37 eV. In this case, the composite ZnMgO NPs bandgap is 3.4 eV.

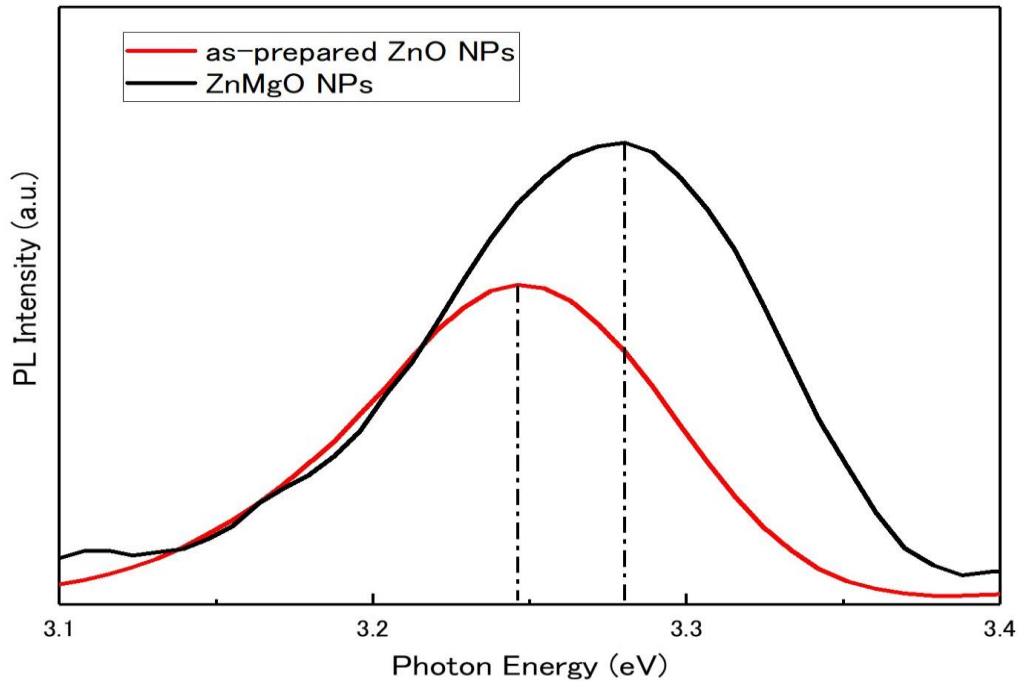


Figure 28. Room temperature photoluminescence spectra of as-prepared ZnO NPs and ZnMgO composite NPs.

5.5 Devices preparation

Two structural LED devices were prepared using N-doped p-type ZnO NPs, and ZnMgO composite NPs coated on the GZO electrode. One LED structure is p-ZnO/GZO, and another is p-ZnO/ZnMgO/GZO, as shown in **Figures 29** (a) and (b). The ZnMgO NPs dispersions with n-type conductivity were prepared by mixing 0.2g ZnMgO composite NPs with 20 ml pure water using an ultrasonic homogenizer. Using a centrifugal separator, the large particles were separated. For creating the ZnMgO NPs layer, the dispersion was sprayed by airbrush onto the GZO electrode film, which was on the hot plate for heat treatment at the temperature of 300 °C.

The p-type ZnO NPs were mixed with Isopropyl Alcohol (IPA) (0.3 ml) and binder (0.1g) (Silsequioxane OX-SQ SI 20, Toagosei Co., Ltd) and placed on the GZO film and

ZnMgO NPs layer by spin coating process for the fabrication of LEDs. Gold (Au) was deposited on the p-ZnO layer and GZO as a contact electrode.

Figure 30 (a) and (b) show the band diagram of LEDs with p-ZnO/GZO and p-ZnO/n-ZnMgO/GZO structures, respectively.

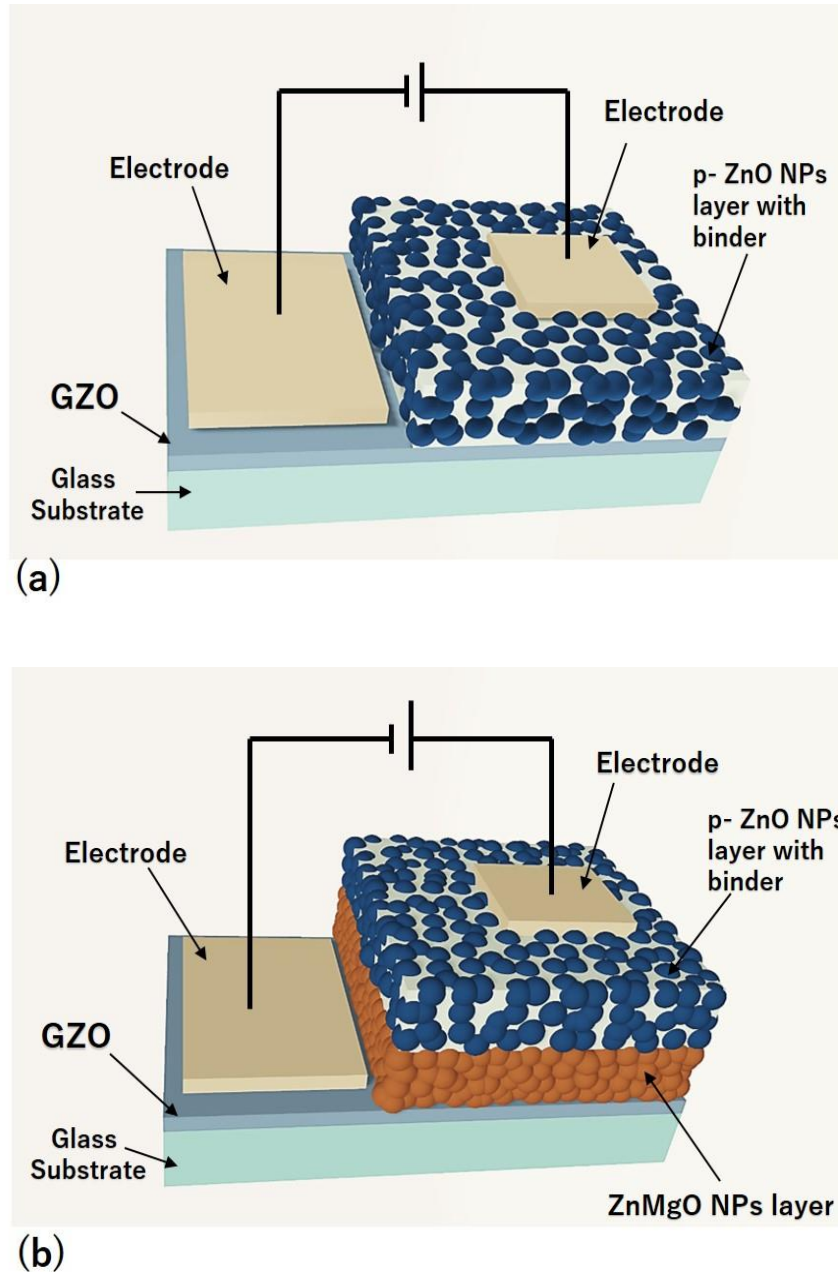


Figure 29. Schematic diagram of ZnO NPs based LEDs. (a) p-ZnO NPs/GZO structure (Reference [49]); (b) p-ZnO NPs/n-ZnMgO NPs/GZO structure.

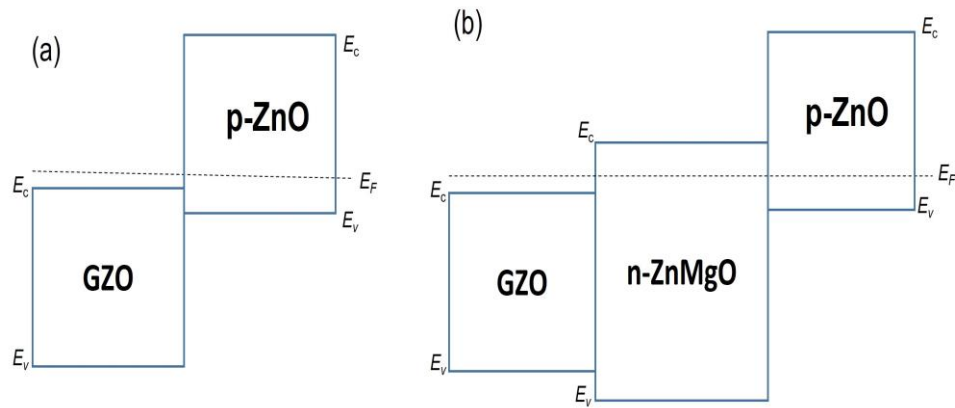


Figure 30. The band diagram of ZnO NPs based LEDs (band bending is not taken into account) (a) p-ZnO/GZO structure; (b) p-ZnO/n-ZnMgO/GZO structure.

5.6 *I-V* Characteristics

The *I-V* properties of these LEDs were evaluated. **Figure 31** shows the *I-V* characteristics of LEDs at room temperature in a dark environment. The leakage current was observed from the *I-V* curve for both structures of LEDs. It can be seen the leakage current reduction was happened for the structure of p-ZnO/n-ZnMgO/GZO LEDs compared to the structure of p-ZnO/GZO LEDs. It seems that the insertion of the ZnMgO NPs composite layer improved the reduction of leakage current in the structure (p-ZnO/n-ZnMgO/GZO) of LED. The reason of the reduction of the leakage was that the barrier layer confined the radiative recombination process in the active region. The *I-V* curve for the LEDs with the structure of p-ZnO/n-ZnMgO/GZO show the turn on voltage of the forward region for p-n junction was similar to the bandgap energy of ZnO, but it was not observed for the LEDs with structure of p-ZnO/GZO due to higher current density compared to the LEDs with structure of p-ZnO/n-ZnMgO/GZO.

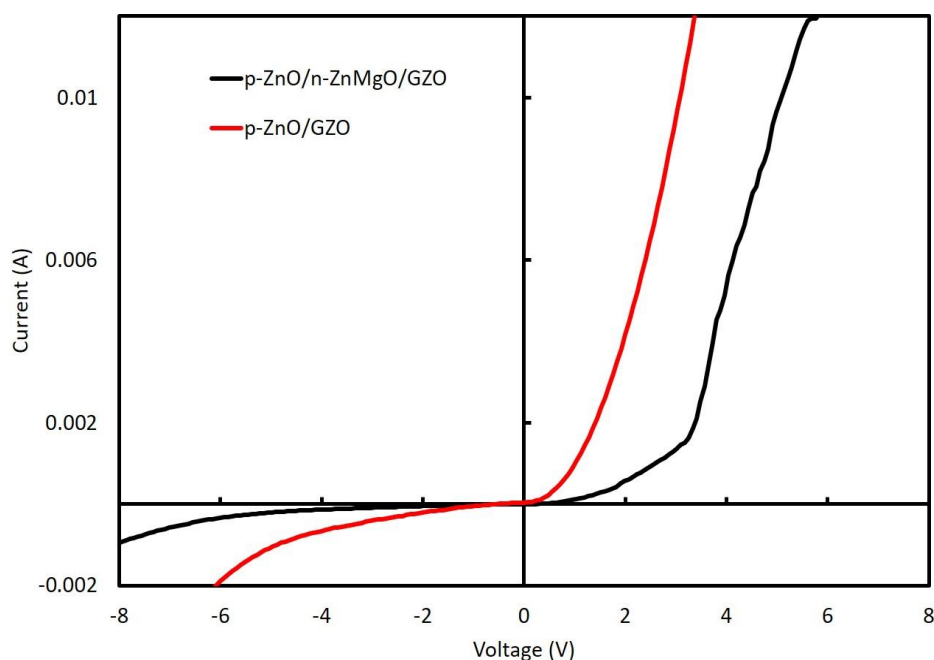


Figure 31. *I-V* characterization of ZnO NPs based LEDs with the structure of p-ZnO/n-ZnMgO/GZO and p-ZnO/GZO.

5.7 EL

The EL spectra of the LEDs with p-ZnO/n-ZnMgO/GZO and p-ZnO/GZO structures at room temperature are presented in **Figure 32**. By inserting the ZnMgO NPs energy barrier layer, the EL spectra intensity increased compared to without the ZnMgO NPs layer. Because GZO has high electron concentration and p-ZnO layer has low hole concentration. The LEDs with p-ZnO/GZO structure shows a charge imbalance, which means that more electrons are congregated in the p-ZnO layer with holes. The configuration of inserting the ZnMgO layer (p-ZnO/n-ZnMgO/GZO) is a structure that balances the concentration of electrons and holes. The reason was that the energy barrier layer blocked the overflow of the holes and accumulated the holes concentration in the active region. **Figure 33** (a) and

(b) show the band diagram of the LEDs with p-ZnO/GZO and p-ZnO/n-ZnMgO/GZO structures under the forward bias conditions, respectively.

The peak energy of EL emission for p-ZnO/GZO LEDs was found at around 3.23 eV. On the other hand, the peak energy of EL spectra for the LED with inserting ZnMgO NPs layer (p-ZnO/n-ZnMgO/GZO) were observed at about 3.21 eV. When comparing the EL spectra for both LEDs, the emission energy peaks were shifted toward the lower energy side. The results prove that the EL emission occurred by the carrier recombination in the p-ZnO NPs layer. The lower direction of peak energy shift is due to the decreased bandgap energy by the heating effect of the rising temperature and increase of carrier density. In this case, for the structure of p-ZnO/GZO LEDs, the carrier will concentrate in the p-ZnO NPs layer with an insulating binder resulting in higher excitation density and redshift. The holes from the p-ZnO NPs layer can flow to GZO, so the carrier density should be lower than that of LED with the ZnMgO NPs layer. On the other hand, the structure of p-ZnO/n-ZnMgO/GZO LEDs contained a ZnMgO NPs layer resulting in temperature raising [83] by the resistivity of the ZnMgO layer, and the large redshift happened. The temperature of the LEDs with the structure of p-ZnO/n-ZnMgO/GZO and p-ZnO/GZO was calculated using the varshni model [83]:

$$E_g(T) = E_g(T=0) - \alpha T^2 / (T + \beta) \quad (6)$$

Where, $E_g(T=0) = 3.44$ eV for ZnO at 0 K [106],[107], the temperature coefficients are, $\alpha = -5.5 \times 10^{-4}$ eVK⁻¹ and $\beta = -900$ K for temperature up to 300 K [86], [87]. The temperature calculated from the peak energy (3.21 eV) of EL spectra for the LEDs with the structure of p-ZnO/n-ZnMgO/GZO was approximately 440 K. On the other hand, the temperature for the peak energy (3.23 eV) of EL spectra for LEDs with the structure of p-ZnO/GZO was approximately 426 K.

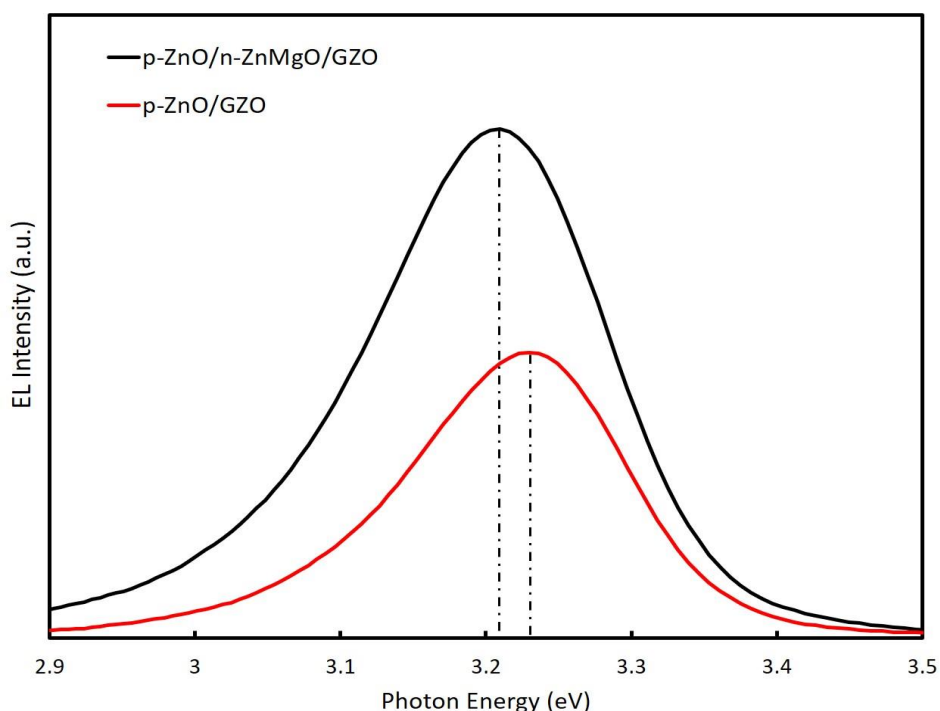


Figure 32. Comparison of EL spectra for ZnO NPs LEDs with the structure of p-ZnO/n-ZnMgO/GZO and p-ZnO/GZO.

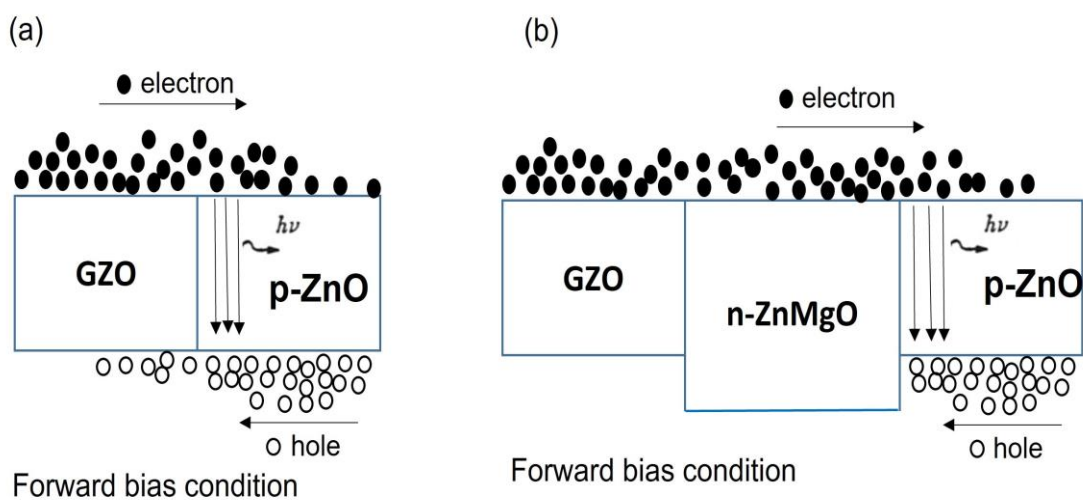


Figure 33. The band diagram of ZnO NPs based LEDs at forward bias condition (band bending is not taken into account) (a) p-ZnO/GZO structure; (b) p-ZnO/n-ZnMgO/GZO structure.

5.8 Conclusion:

The bandgap engineering of ZnO NPs confirmed by the compositing with MgO NPs. The characterization of the composite ZnMgO NPs was revealed by changing the peak energy of the optical emission. The ZnMgO NPs included in the ZnO-based LEDs as an energy barrier layer, which created the carrier confinement of the radiative recombination in the active region of the devices. The leakage current of the LEDs with the structure of p-ZnO/n-ZnMgO/GZO was reduced as well as the EL emission increased compared to the LEDs with the structure of p-ZnO/GZO by confining the carrier recombination.

6. Summary

To develop the LED based on ZnO, this study provides new knowledge about analysis and understanding of the role of N-dopants in ZnO NPs. The DC arc plasma gas evaporation method was applied to synthesize the efficient acceptor N-doped ZnO NPs. The obtaining p-type and n-type conductivity of ZnO NPs was followed different chamber pressure and arc current conditions. The local vibrational modes (LVM) of Raman spectra confirmed the nitrogen concentration in the ZnO NPs crystal. The PL spectra were conducted to observe the optical emission of these ZnO NPs. The observation of band edge emission of PL confirmed the dominance of acceptor nitrogen in ZnO NPs crystals. The donor-acceptor pair emission showed the acceptor concentration in the ZnO NPs crystal, which had a linear proportion with the 275 cm^{-1} peaks of Raman spectra of the ZnO NPs. The p-type ZnO NPs were used to fabricate LEDs as a p-type layer. The LEDs exhibited the diode rectifying behavior of *I-V* characteristics and ultraviolet emission from EL measurement. The LEDs' demonstration confirmed that the p-type conductivity of the ZnO NPs layer acted as a hole injection layer.

N-doped p-type and Ga-doped n-type ZnO NPs used to fabricate the UV homo-junction LEDs. By concluding the experimental results, including electrical and spectral evaluation, it can be confirmed that the hole was injected from the p-type layer to the n-type layer. The LEDs acted as a p-n homo-junction devices. The attempt of p-type and n-type ZnO NPs based homo-junction UV LEDs is the world's first demonstration.

It was successfully prepared the ZnMgO composite NPs. The results of the characterization of ZnMgO NPs were revealed good characteristics. By adding the ZnMgO composite NPs layer as a barrier layer in the diodes, the LEDs' leakage current was reduced,

and the EL emission of the diodes increased by balancing the carrier radiative recombination.

In general, the presents research work has a significant novelty and practical relevance. The motivation and methodological details were presented comprehensively and systematically. This research work offers new practical knowledge and technology relevant. The results may help for the development of future technologies as well as LED efficiently and beneficially.

7. Future tasks

1. It requires the quality and reproducibility of nitrogen doped ZnO NPs by optimizing some conditions.
2. Gallium-doped ZnO NPs require optimization conditions and improve the characterization of the Ga-doped ZnO NPs.
3. ZnMgO composite NPs require optimization conditions and improve the characteristic performance of the ZnMgO NPs.
4. All devices fabrication processes need to optimize some conditions and improve the device's performance. Enhancing the emission of the devices can be possible for practical use in the future.

Reference

- [1] “advanced-physicsprize2014.pdf.”
- [2] S. Nakamura, M. Senoh, and T. Mukai, “High-power InGaN/GaN double-heterostructure violet light emitting diodes,” *Appl. Phys. Lett.*, vol. 62, no. 19, pp. 2390–2392, May 1993, doi: 10.1063/1.109374.
- [3] S. Inoue, T. Naoki, T. Kinoshita, T. Obata, and H. Yanagi, “Light extraction enhancement of 265 nm deep-ultraviolet light-emitting diodes with over 90 mW output power via an AlN hybrid nanostructure,” *Appl. Phys. Lett.*, vol. 106, no. 13, p. 131104, Mar. 2015, doi: 10.1063/1.4915255.
- [4] S. Nakamura, T. M. T. Mukai, and M. S. M. Senoh, “High-Power GaN P-N Junction Blue-Light-Emitting Diodes,” *Jpn. J. Appl. Phys.*, vol. 30, no. 12A, p. L1998, Dec. 1991, doi: 10.1143/JJAP.30.L1998.
- [5] “Light Emitting Diode (LED) - Working, Construction and Symbol - Diode.” <https://www.physics-and-radio-electronics.com/electronic-devices-and-circuits/semiconductor-diodes/lightemittingdiodeledconstructionworking.html> (accessed Jan. 20, 2022).
- [6] A. Janotti and C. G. Van de Walle, “Fundamentals of zinc oxide as a semiconductor,” *Rep. Prog. Phys.*, vol. 72, no. 12, p. 126501, Dec. 2009, doi: 10.1088/0034-4885/72/12/126501.
- [7] Y.-S. Choi, J.-W. Kang, D.-K. Hwang, and S.-J. Park, “Recent Advances in ZnO-Based Light-Emitting Diodes,” *IEEE Trans. Electron Devices*, vol. 57, no. 1, pp. 26–41, Jan. 2010, doi: 10.1109/TED.2009.2033769.
- [8] Ü. Özgür, D. Hofstetter, and H. Morkoç, “ZnO Devices and Applications: A Review of Current Status and Future Prospects,” *Proc. IEEE*, vol. 98, no. 7, pp. 1255–1268, Jul. 2010, doi: 10.1109/JPROC.2010.2044550.
- [9] D. Look, “Recent Advances in ZnO Materials and Devices,” *Mater. Sci. Eng. B-Solid State Mater. Adv. Technol.*, vol. 80, no. 1–3, pp. 383–387, Jan. 2001, doi: 10.1016/S0921-5107(00)00604-8.
- [10] J. Hu and R. G. Gordon, “Textured aluminum-doped zinc oxide thin films from atmospheric pressure chemical-vapor deposition,” *J. Appl. Phys.*, vol. 71, no. 2, pp. 880–890, Jan. 1992, doi: 10.1063/1.351309.
- [11] H. J. Ko, Y. F. Chen, S. K. Hong, H. Wensch, T. Yao, and D. C. Look, “Ga-doped ZnO films grown on GaN templates by plasma-assisted molecular-beam epitaxy,” *Appl. Phys. Lett.*, vol. 77, no. 23, pp. 3761–3763, Dec. 2000, doi: 10.1063/1.1331089.

- [12] J. Hu and R. G. Gordon, “Electrical and Optical Properties of Indium Doped Zinc Oxide Films Prepared by Atmospheric Pressure Chemical Vapor Deposition,” *MRS Online Proc. Libr. OPL*, vol. 283, ed 1992, doi: 10.1557/PROC-283-891.
- [13] “Electrical and optical properties of boron-doped ZnO thin films for solar cells grown by metalorganic chemical vapor deposition: Journal of Applied Physics: Vol 70, No 11.” <https://aip.scitation.org/doi/abs/10.1063/1.349794> (accessed Nov. 12, 2021).
- [14] O. Maksimov, “RECENT ADVANCES AND NOVEL APPROACHES OF P-TYPE DOPING OF ZINC OXIDE,” p. 9.
- [15] J.-H. Lim, C.-K. Kang, K.-K. Kim, I.-K. Park, D.-K. Hwang, and S.-J. Park, “UV Electroluminescence Emission from ZnO Light-Emitting Diodes Grown by High-Temperature Radiofrequency Sputtering,” *Adv. Mater.*, vol. 18, no. 20, pp. 2720–2724, Oct. 2006, doi: 10.1002/adma.200502633.
- [16] S. Chu, J. H. Lim, L. J. Mandalapu, Z. Yang, L. Li, and J. L. Liu, “Sb-doped p-ZnO/Ga-doped n-ZnO homojunction ultraviolet light emitting diodes,” *Appl. Phys. Lett.*, vol. 92, no. 15, p. 152103, Apr. 2008, doi: 10.1063/1.2908968.
- [17] S. Limpijumnong, S. B. Zhang, S.-H. Wei, and C. H. Park, “Doping by Large-Size-Mismatched Impurities: The Microscopic Origin of Arsenic- or Antimony-Doped p-Type Zinc Oxide,” *Phys. Rev. Lett.*, vol. 92, no. 15, p. 155504, Apr. 2004, doi: 10.1103/PhysRevLett.92.155504.
- [18] D. C. Look, “Progress in ZnO materials and devices,” *J. Electron. Mater.*, vol. 35, no. 6, pp. 1299–1305, Jun. 2006, doi: 10.1007/s11664-006-0258-y.
- [19] K. M. K. Minegishi, Y. K. Y. Koiwai, Y. K. Y. Kikuchi, K. Y. K. Yano, M. K. M. Kasuga, and A. S. A. Shimizu, “Growth of p-type Zinc Oxide Films by Chemical Vapor Deposition,” *Jpn. J. Appl. Phys.*, vol. 36, no. 11A, p. L1453, Nov. 1997, doi: 10.1143/JJAP.36.L1453.
- [20] B. K. Meyer *et al.*, “Bound exciton and donor–acceptor pair recombinations in ZnO,” *Phys. Status Solidi B*, vol. 241, no. 2, pp. 231–260, 2004, doi: 10.1002/pssb.200301962.
- [21] H. Maki *et al.*, “Nitrogen Ion Behavior on Polar Surfaces of ZnO Single Crystals,” *Jpn. J. Appl. Phys.*, vol. 42, no. 1R, p. 75, Jan. 2003, doi: 10.1143/JJAP.42.75.
- [22] M. Joseph, H. Tabata, and T. Kawai, “p-Type Electrical Conduction in ZnO Thin Films by Ga and N Codoping,” *Jpn. J. Appl. Phys.*, vol. 38, no. 11A, p. L1205, Nov. 1999, doi: 10.1143/JJAP.38.L1205.

- [23] Y. Fujita *et al.*, “Near ultraviolet light emitting diodes using ZnMgO:N/ZnO hetero-junction grown by MOVPE,” *J. Cryst. Growth*, vol. 464, pp. 226–230, Apr. 2017, doi: 10.1016/j.jcrysgro.2016.10.085.
- [24] H. Amano, M. Kito, K. Hiramatsu, and I. Akasaki, “P-Type Conduction in Mg-Doped GaN Treated with Low-Energy Electron Beam Irradiation (LEEBI),” *Jpn. J. Appl. Phys.*, vol. 28, no. 12A, p. L2112, Dec. 1989, doi: 10.1143/JJAP.28.L2112.
- [25] H. C. Chen *et al.*, “White-Light Electroluminescence From n-ZnO/p-GaN Heterojunction Light-Emitting Diodes at Reverse Breakdown Bias,” *IEEE Trans. Electron Devices*, vol. 58, no. 11, pp. 3970–3975, Nov. 2011, doi: 10.1109/TED.2011.2164408.
- [26] J. Kong, S. Chu, M. Olmedo, L. Li, Z. Yang, and J. Liu, “Dominant ultraviolet light emissions in packed ZnO columnar homojunction diodes,” *Appl. Phys. Lett.*, vol. 93, no. 13, p. 132113, Sep. 2008, doi: 10.1063/1.2992629.
- [27] K. Nakahara *et al.*, “Nitrogen doped Mg_xZn_{1-x}O/ZnO single heterostructure ultraviolet light-emitting diodes on ZnO substrates,” *Appl. Phys. Lett.*, vol. 97, no. 1, p. 013501, Jul. 2010, doi: 10.1063/1.3459139.
- [28] A. Tsukazaki *et al.*, “Repeated temperature modulation epitaxy for p-type doping and light-emitting diode based on ZnO,” *Nat. Mater.*, vol. 4, no. 1, Art. no. 1, Jan. 2005, doi: 10.1038/nmat1284.
- [29] A. Chen *et al.*, “Beryllium-Assisted p-Type Doping for ZnO Homojunction Light-Emitting Devices,” *Adv. Funct. Mater.*, vol. 26, no. 21, pp. 3696–3702, Jun. 2016, doi: 10.1002/adfm.201600163.
- [30] A. Dadgar *et al.*, “Heteroepitaxy and nitrogen doping of high-quality ZnO,” *J. Cryst. Growth*, vol. 272, no. 1, pp. 800–804, Dec. 2004, doi: 10.1016/j.jcrysgro.2004.08.030.
- [31] S. Heinze *et al.*, “Homoepitaxial growth of ZnO by metalorganic vapor phase epitaxy in two-dimensional growth mode,” *J. Cryst. Growth*, vol. 308, pp. 170–175, Oct. 2007, doi: 10.1016/j.jcrysgro.2007.07.024.
- [32] E. Fujimoto *et al.*, “Hetero-Epitaxial Growth of ZnO Film by Temperature-Modulated Metalorganic Chemical Vapor Deposition,” *Appl. Phys. Express*, vol. 2, no. 4, p. 045502, Apr. 2009, doi: 10.1143/APEX.2.045502.
- [33] F. Quaranta, A. Valentini, F. R. Rizzi, and G. Casamassima, “Dual-ion-beam sputter deposition of ZnO films,” *J. Appl. Phys.*, vol. 74, no. 1, pp. 244–248, Jul. 1993, doi: 10.1063/1.354152.
- [34] D. C. Look *et al.*, “Electrical properties of bulk ZnO,” *Solid State Commun.*, vol. 105, no. 6, pp. 399–401, Feb. 1998, doi: 10.1016/S0038-1098(97)10145-4.

- [35] K. Pradeev Raj, K. Sadaiyandi, A. Kennedy, and R. Thamizselvi, “Structural, optical, photoluminescence and photocatalytic assessment of Sr-doped ZnO nanoparticles,” *Mater. Chem. Phys.*, vol. 183, pp. 24–36, Nov. 2016, doi: 10.1016/j.matchemphys.2016.07.068.
- [36] A. Alexandrov, M. Zvaigzne, D. Lypenko, I. Nabiev, and P. Samokhvalov, “Al-, Ga-, Mg-, or Li-doped zinc oxide nanoparticles as electron transport layers for quantum dot light-emitting diodes,” *Sci. Rep.*, vol. 10, no. 1, p. 7496, Dec. 2020, doi: 10.1038/s41598-020-64263-2.
- [37] T. Yoshida, I. M. Maruful, and Y. Fujita, “Trial of Ga-doping on ZnO Nanoparticles by Thermal Treatment with Ga₂O₃ Nanoparticles,” *E-J. Surf. Sci. Nanotechnol.*, vol. 18, pp. 12–17, 2020, doi: 10.1380/ejssnt.2020.12.
- [38] Y. Hiragino *et al.*, “Synthesis of nitrogen-doped ZnO nanoparticles by RF thermal plasma,” *Solid-State Electron.*, vol. 118, pp. 41–45, Apr. 2016, doi: 10.1016/j.sse.2016.01.003.
- [39] B. Chavillon *et al.*, “P-Type Nitrogen-Doped ZnO Nanoparticles Stable under Ambient Conditions,” *J. Am. Chem. Soc.*, vol. 134, no. 1, pp. 464–470, Jan. 2012, doi: 10.1021/ja208044k.
- [40] Q. Ou, K. Shinji, A. Ogino, and M. Nagatsu, “Enhanced photoluminescence of nitrogen-doped ZnO nanoparticles fabricated by Nd:YAG laser ablation,” *J. Phys. D: Appl. Phys.*, vol. 41, no. 20, p. 205104, Sep. 2008, doi: 10.1088/0022-3727/41/20/205104.
- [41] T. Yi-hao, Z. Hang, W. Yin, D. Ming-hui, J. Guo, and Z. Bin, “Facile fabrication of nitrogen-doped zinc oxide nanoparticles with enhanced photocatalytic performance,” *Micro Nano Lett.*, vol. 10, no. 9, pp. 432–434, Sep. 2015, doi: 10.1049/mnl.2015.0130.
- [42] K. Senthilkumar, O. Senthilkumar, S. Morito, T. Ohba, and Y. Fujita, “Synthesis of zinc oxide nanoparticles by dc arc dusty plasma,” *J. Nanoparticle Res.*, vol. 14, no. 10, p. 1205, Oct. 2012, doi: 10.1007/s11051-012-1205-x.
- [43] O. Senthilkumar, K. Yamauchi, K. Senthilkumar, T. Yamamae, and Y. F. and N. Nishimoto, “UV-Blue Light Emission from ZnO Nanoparticles,” *J. Korean Phys. Soc.*, vol. 53, no. 1, pp. 46–49, Jul. 2008, doi: 10.3938/jkps.53.46.
- [44] K. Senthilkumar *et al.*, “Multiphonon scattering and non-radiative decay in ZnO nanoparticles,” *Phys. Status Solidi C*, vol. 7, no. 6, pp. 1586–1588, Mar. 2010, doi: 10.1002/pssc.200983203.

- [45] E. Neshataeva, T. Kümmell, G. Bacher, and A. Ebberts, “All-inorganic light emitting device based on ZnO nanoparticles,” *Appl. Phys. Lett.*, vol. 94, no. 9, p. 091115, Mar. 2009, doi: 10.1063/1.3093675.
- [46] D. Itohara, K. Shinohara, T. Yoshida, and Y. Fujita, “p-Channel and n-Channel Thin-Film-Transistor Operation on Sprayed ZnO Nanoparticle Layers,” *J. Nanomater.*, vol. 2016, p. e8219326, Aug. 2016, doi: 10.1155/2016/8219326.
- [47] Y. Fujita, K. Moriyama, Y. Hiragino, Y. Furubayashi, H. Hashimoto, and T. Yoshida, “Electroluminescence from nitrogen doped ZnO nanoparticles,” *Phys. Status Solidi C*, vol. 11, no. 7–8, pp. 1260–1262, 2014, doi: <https://doi.org/10.1002/pssc.201300645>.
- [48] I. M. Shafiqul, R. Deep, J. Lin, T. Yoshida, and Y. Fujita, “Demonstration and Evaluation of p-Type and n-Type ZnO Nanoparticles-Based Homojunction UV Light-Emitting Diodes,” *Phys. Status Solidi RRL – Rapid Res. Lett.*, vol. n/a, no. n/a, p. 2100556, doi: 10.1002/pssr.202100556.
- [49] I. M. Shafiqul, R. Deep, J. Lin, T. Yoshida, and Y. Fujita, “The Role of Nitrogen Dopants in ZnO Nanoparticle-Based Light Emitting Diodes,” *Nanomaterials*, vol. 12, no. 3, Art. no. 3, Jan. 2022, doi: 10.3390/nano12030358.
- [50] H. W. Kunert, D. J. Brink, F. D. Auret, J. Malherbe, J. Barnas, and V. Kononenko, “Multiphonon processes in ZnO,” *Phys. Status Solidi C*, vol. 2, no. 3, pp. 1131–1136, Feb. 2005, doi: 10.1002/pssc.200460674.
- [51] C. Bundesmann *et al.*, “Raman scattering in ZnO thin films doped with Fe, Sb, Al, Ga, and Li,” *Appl. Phys. Lett.*, vol. 83, no. 10, pp. 1974–1976, Sep. 2003, doi: 10.1063/1.1609251.
- [52] D. J. Geurts and D. R. Neder, “Eingereicht im Oktober 2008 bei der Fakultät für Physik und Astronomie,” p. 193.
- [53] R. Cuscó *et al.*, “Temperature dependence of Raman scattering in ZnO,” *Phys. Rev. B*, vol. 75, no. 16, p. 165202, Apr. 2007, doi: 10.1103/PhysRevB.75.165202.
- [54] J. M. Calleja and M. Cardona, “Resonant Raman scattering in ZnO,” *Phys. Rev. B*, vol. 16, no. 8, pp. 3753–3761, Oct. 1977, doi: 10.1103/PhysRevB.16.3753.
- [55] A. Kaschner *et al.*, “Nitrogen-related local vibrational modes in ZnO:N,” *Appl. Phys. Lett.*, vol. 80, no. 11, pp. 1909–1911, Mar. 2002, doi: 10.1063/1.1461903.
- [56] “nanomaterials-1552041 revised final version.pdf.”
- [57] F. Friedrich, M. A. Gluba, and N. H. Nickel, “Identification of nitrogen and zinc related vibrational modes in ZnO,” *Appl. Phys. Lett.*, vol. 95, no. 14, p. 141903, Oct. 2009, doi: 10.1063/1.3243454.

- [58] C. Klingshirn, "ZnO: From basics towards applications," *Phys. Status Solidi B*, vol. 244, no. 9, pp. 3027–3073, Sep. 2007, doi: 10.1002/pssb.200743072.
- [59] V. Gupta and A. Mansingh, "Influence of postdeposition annealing on the structural and optical properties of sputtered zinc oxide film," *J. Appl. Phys.*, vol. 80, no. 2, pp. 1063–1073, Jul. 1996, doi: 10.1063/1.362842.
- [60] S. A. Studenikin, N. Golego, and M. Cocivera, "Fabrication of green and orange photoluminescent, undoped ZnO films using spray pyrolysis," *J. Appl. Phys.*, vol. 84, no. 4, pp. 2287–2294, Aug. 1998, doi: 10.1063/1.368295.
- [61] L. Schmidt-Mende and J. L. MacManus-Driscoll, "ZnO – nanostructures, defects, and devices," *Mater. Today*, vol. 10, no. 5, pp. 40–48, May 2007, doi: 10.1016/S1369-7021(07)70078-0.
- [62] Y. G. Wang, S. P. Lau, X. H. Zhang, H. W. Lee, H. H. Hng, and B. K. Tay, "Observations of nitrogen-related photoluminescence bands from nitrogen-doped ZnO films," *J. Cryst. Growth*, vol. 252, no. 1–3, pp. 265–269, May 2003, doi: 10.1016/S0022-0248(03)00878-9.
- [63] S. Yamauchi, Y. Goto, and T. Hariu, "Photoluminescence studies of undoped and nitrogen-doped ZnO layers grown by plasma-assisted epitaxy," *J. Cryst. Growth*, vol. 260, no. 1, pp. 1–6, Jan. 2004, doi: 10.1016/j.jcrysgro.2003.08.002.
- [64] F. Reuss *et al.*, "Optical investigations on the annealing behavior of gallium- and nitrogen-implanted ZnO," *J. Appl. Phys.*, vol. 95, no. 7, pp. 3385–3390, Apr. 2004, doi: 10.1063/1.1650899.
- [65] K. Tamura *et al.*, "Donor–acceptor pair luminescence in nitrogen-doped ZnO films grown on lattice-matched ScAlMgO₄ (0001) substrates," *Solid State Commun.*, vol. 127, no. 4, pp. 265–269, Jul. 2003, doi: 10.1016/S0038-1098(03)00424-1.
- [66] J. G. Reynolds *et al.*, "Shallow acceptor complexes in p-type ZnO," *Appl. Phys. Lett.*, vol. 102, no. 15, p. 152114, Apr. 2013, doi: 10.1063/1.4802753.
- [67] A. Zeuner *et al.*, "Nitrogen doping in bulk and epitaxial ZnO," *Phys. Status Solidi C*, vol. 1, no. 4, pp. 731–734, 2004, doi: 10.1002/pssc.200304255.
- [68] K. Ando *et al.*, "Structural instability of N-acceptors in homo- and heteroepitaxially grown ZnO by MBE," *Phys. Status Solidi B*, vol. 247, no. 6, pp. 1453–1456, 2010, doi: 10.1002/pssb.200983208.
- [69] K. Senthilkumar, O. Senthilkumar, S. Morito, T. Ohba, and Y. Fujita, "Synthesis of zinc oxide nanoparticles by dc arc dusty plasma," *J. Nanoparticle Res.*, vol. 14, no. 10, p. 1205, Sep. 2012, doi: 10.1007/s11051-012-1205-x.

- [70] Y. X. Liu *et al.*, “Preferred orientation of ZnO nanoparticles formed by post-thermal annealing zinc implanted silica,” *Solid State Commun.*, vol. 121, no. 9–10, pp. 531–536, Mar. 2002, doi: 10.1016/S0038-1098(02)00006-6.
- [71] H. Gómez and M. de la L. Olvera, “Ga-doped ZnO thin films: Effect of deposition temperature, dopant concentration, and vacuum-thermal treatment on the electrical, optical, structural and morphological properties,” *Mater. Sci. Eng. B*, vol. 134, no. 1, pp. 20–26, Sep. 2006, doi: 10.1016/j.mseb.2006.07.039.
- [72] K. Ozaki and M. Gomi, “Strong Ultraviolet Photoluminescence in Polycrystalline ZnO Sputtered Films,” *Jpn. J. Appl. Phys.*, vol. 41, no. Part 1, No. 9, pp. 5614–5617, Sep. 2002, doi: 10.1143/JJAP.41.5614.
- [73] J. Lim, K. Shin, H. Woo Kim, and C. Lee, “Photoluminescence Studies of ZnO thin films grown by atomic layer epitaxy,” *J. Lumin.*, vol. 109, no. 3, pp. 181–185, Sep. 2004, doi: 10.1016/j.jlumin.2004.02.006.
- [74] “McCluskey and Jokela - APPLIED PHYSICS REVIEWS—FOCUSED REVIEW.pdf.”
- [75] H. Kato, M. Sano, K. Miyamoto, and T. Yao, “Growth and characterization of Ga-doped ZnO layers on a-plane sapphire substrates grown by molecular beam epitaxy,” *J. Cryst. Growth*, vol. 237–239, pp. 538–543, Apr. 2002, doi: 10.1016/S0022-0248(01)01972-8.
- [76] J. Cho *et al.*, “Enhancement of Photoluminescence and Electrical Properties of Ga-Doped ZnO Thin Film Grown on α -Al₂O₃(0001) Single-Crystal Substrate by rf Magnetron Sputtering through Rapid Thermal Annealing,” vol. 40, no. 10, p. 5, 2001.
- [77] W. Zhu *et al.*, “Analysis of defect luminescence in Ga-doped ZnO nanoparticles,” *Phys. Chem. Chem. Phys. PCCP*, vol. 18, no. 14, pp. 9586–9593, Apr. 2016, doi: 10.1039/c6cp00746e.
- [78] M. Schirra *et al.*, “Acceptor-related luminescence at 3.314eV in zinc oxide confined to crystallographic line defects,” *Phys. B Condens. Matter*, vol. 401–402, pp. 362–365, Dec. 2007, doi: 10.1016/j.physb.2007.08.188.
- [79] L.-C. Chao, J.-W. Chen, H.-C. Peng, and C.-H. Ho, “Characterization of nitrogen doped p-type ZnO thin films prepared by reactive ion beam sputter deposition,” *Surf. Coat. Technol.*, vol. 231, pp. 492–495, Sep. 2013, doi: 10.1016/j.surfcoat.2012.10.077.
- [80] T. K. Pathak, V. Kumar, H. C. Swart, and L. P. Purohit, “Effect of doping concentration on the conductivity and optical properties of p-type ZnO thin films,” *Phys. B Condens. Matter*, vol. 480, pp. 31–35, Jan. 2016, doi: 10.1016/j.physb.2015.09.033.

- [81] X. Nie, B. Zhang, J. Wang, L. Shi, Z. Di, and Q. Guo, "Room-temperature ferromagnetism in p-type nitrogen-doped ZnO films," *Mater. Lett.*, vol. 161, pp. 355–359, Dec. 2015, doi: 10.1016/j.matlet.2015.08.143.
- [82] S. W. Lee *et al.*, "Origin of forward leakage current in GaN-based light-emitting devices," *Appl. Phys. Lett.*, vol. 89, no. 13, p. 132117, Sep. 2006, doi: 10.1063/1.2357930.
- [83] Y. P. Varshni, "Temperature dependence of the energy gap in semiconductors," *Physica*, vol. 34, no. 1, pp. 149–154, Jan. 1967, doi: 10.1016/0031-8914(67)90062-6.
- [84] A. Yamamoto, T. Kido, T. Goto, Y. Chen, and T. Yao, "Bandgap renormalization of ZnO epitaxial thin films," *Solid State Commun.*, p. 4, 2002.
- [85] H. Kong, "ULTRAVIOLET SPONTANEOUS AND STIMULATED EMISSIONS FROM ZnO MICROCRYSTALLITE THIN FILMS AT ROOM TEMPERATURE P. Zu," Z.K. Tang," G.K.L. Wong," M. Kawasaki,* A. Ohtomo,b H. Koinuma' and Y. Segawad," vol. 103, no. 8, p. 5.
- [86] H. Morkoç and Ü. Özgür, *Zinc Oxide: Fundamentals, Materials and Device Technology*. John Wiley & Sons, 2008.
- [87] "Landolt-Börnstein: Numerical Data and Functional Relationships in Science and Technology - New Series | Book series home." <https://www.springer.com/series/284> (accessed Jan. 26, 2022).
- [88] N. B. Chen and C. H. Sui, "Recent progress in research on $Mg_xZn_{1-x}O$ alloys," *Mater. Sci. Eng. B*, vol. 126, no. 1, pp. 16–21, Jan. 2006, doi: 10.1016/j.mseb.2005.08.112.
- [89] Q. Zhang *et al.*, "ZnMgO:ZnO composite films for fast electron transport and high charge balance in quantum dot light emitting diodes," *Opt. Mater. Express*, vol. 8, no. 4, pp. 909–918, Apr. 2018, doi: 10.1364/OME.8.000909.
- [90] Y.-S. Choi, J.-W. Kang, B.-H. Kim, D.-K. Na, S.-J. Lee, and S.-J. Park, "Improved electroluminescence from ZnO light-emitting diodes by p-type MgZnO electron blocking layer," *Opt. Express*, vol. 21, no. 10, p. 11698, May 2013, doi: 10.1364/OE.21.011698.
- [91] J. Pan *et al.*, "Size Tunable ZnO Nanoparticles To Enhance Electron Injection in Solution Processed QLEDs," *ACS Photonics*, vol. 3, no. 2, pp. 215–222, Feb. 2016, doi: 10.1021/acsp Photonics.5b00267.
- [92] I. Cho *et al.*, "Multifunctional Dendrimer Ligands for High-Efficiency, Solution-Processed Quantum Dot Light-Emitting Diodes," *ACS Nano*, vol. 11, no. 1, pp. 684–692, Jan. 2017, doi: 10.1021/acsnano.6b07028.

- [93] S. Cao *et al.*, “Enhancing the Performance of Quantum Dot Light-Emitting Diodes Using Room-Temperature-Processed Ga-Doped ZnO Nanoparticles as the Electron Transport Layer,” *ACS Appl. Mater. Interfaces*, vol. 9, no. 18, pp. 15605–15614, May 2017, doi: 10.1021/acsami.7b03262.
- [94] S. Wang *et al.*, “Bandgap tunable Zn_{1-x}Mg_xO thin films as electron transport layers for high performance quantum dot light-emitting diodes,” *J. Mater. Chem. C*, vol. 5, no. 19, pp. 4724–4730, May 2017, doi: 10.1039/C7TC00453B.
- [95] A. W. Cohn, K. R. Kittilstved, and D. R. Gamelin, “Tuning the Potentials of ‘Extra’ Electrons in Colloidal n-Type ZnO Nanocrystals via Mg²⁺ Substitution,” *J. Am. Chem. Soc.*, vol. 134, no. 18, pp. 7937–7943, May 2012, doi: 10.1021/ja3019934.
- [96] X. Qiu, L. Li, J. Zheng, J. Liu, X. Sun, and G. Li, “Origin of the Enhanced Photocatalytic Activities of Semiconductors: A Case Study of ZnO Doped with Mg²⁺,” *J. Phys. Chem. C*, vol. 112, no. 32, pp. 12242–12248, Aug. 2008, doi: 10.1021/jp803129e.
- [97] Mohd. Arshad *et al.*, “Band gap engineering and enhanced photoluminescence of Mg doped ZnO nanoparticles synthesized by wet chemical route,” *J. Lumin.*, vol. 161, pp. 275–280, May 2015, doi: 10.1016/j.jlumin.2014.12.016.
- [98] D. C. Olson *et al.*, “Band-Offset Engineering for Enhanced Open-Circuit Voltage in Polymer–Oxide Hybrid Solar Cells,” *Adv. Funct. Mater.*, vol. 17, no. 2, pp. 264–269, 2007, doi: 10.1002/adfm.200600215.
- [99] L. S. Rao, T. V. Rao, Sd. Naheed, and P. V. Rao, “Structural and optical properties of zinc magnesium oxide nanoparticles synthesized by chemical co-precipitation,” *Mater. Chem. Phys.*, vol. 203, pp. 133–140, Jan. 2018, doi: 10.1016/j.matchemphys.2017.09.048.
- [100] A. R. Denton and N. W. Ashcroft, “Vegard’s law,” *Phys. Rev. A*, vol. 43, no. 6, pp. 3161–3164, Mar. 1991, doi: 10.1103/PhysRevA.43.3161.
- [101] Hiroyoshi Momida and Tamio Oguchi 2018 *Appl. Phys. Express* **11** 041201
- [102] Vashaei *et al.* *J. Appl. Phys.* **98**, 054911 (2005).
- [103] A. S. Ahmed, M. Shafeeq M., M. L. Singla, S. Tabassum, A. H. Naqvi, and A. Azam, “Band gap narrowing and fluorescence properties of nickel doped SnO₂ nanoparticles,” *J. Lumin.*, vol. 131, no. 1, pp. 1–6, Jan. 2011, doi: 10.1016/j.jlumin.2010.07.017.
- [104] T. Takagahara and K. Takeda, “Theory of the quantum confinement effect on excitons in quantum dots of indirect-gap materials,” *Phys. Rev. B*, vol. 46, no. 23, pp. 15578–15581, Dec. 1992, doi: 10.1103/PhysRevB.46.15578.

- [105] I. Hamberg and C. G. Granqvist, "BANDGAP WIDENING IN HEAVILY DOPED OXIDE SEMICONDUCTORS USED AS TRANSPARENT HEAT-REFLECTORS," p. 12.
- [106] A. Janotti, D. Segev, and C. G. Van de Walle, "Effects of cation d states on the structural and electronic properties of III-nitride and II-oxide wide-band-gap semiconductors," *Phys. Rev. B*, vol. 74, no. 4, p. 045202, Jul. 2006, doi: 10.1103/PhysRevB.74.045202.
- [107] "Semiconductor Band Gaps." <http://hyperphysics.phy-astr.gsu.edu/hbase/Tables/Semgap.html> (accessed Jan. 26, 2022).

List of Publications

List of Articles Publication in Journal:

1. **Islam Mohammad Shafiqul**, Raj Deep, Jie Lin, Toshiyuki Yoshida and Yasuhisa Fujita. “Demonstration and Evaluation of p-Type and n-Type ZnO Nanoparticles-Based Homojunction UV Light-Emitting Diodes”. *physica status solidi (RRL)- Rapid Research Letter*. 2100556 <https://doi.org/10.1002/pssr.202100556>.
2. **Islam Mohammad Shafiqul**, Raj Deep, Jie Lin, Toshiyuki Yoshida and Yasuhisa Fujita. “The Role of Nitrogen Dopants in ZnO Nanoparticle-Based Light Emitting Diodes”. *Nanomaterials* 2022, 12 (3), 358. <https://doi.org/10.3390/nano12030358>.

List of Conference Presentation (Author):

1. **Islam Mohammad Shafiqul**, Yuki Konishi, Raj Deep, Jie Lin, Toshiyuki Yoshida, Yasuhisa Fujita, “The Emission Power of ZnO Nanoparticle-based LEDs enhanced by adding Silica nanoparticles.” JSAP spring meeting 2021, **Oral presentation** (Abstract/ program no- 18p-Z33-3).
2. **Islam Mohammad Shafiqul**, Yuki Konishi, Raj Deep, Jie Lin, Toshiyuki Yoshida, Yasuhisa Fujita, “The Electroluminescence of ZnO nanoparticle-based LEDs improved by inserting a ZnMgO nanoparticles layer.” JSAP spring meeting 2021, **Oral presentation** (Abstract/ program no- 18p-Z33-4).
3. **Islam Mohammad Shafiqul**, A. Tabuchi, Y. Konishi, C. Sakurai, J. Lin, T. Yoshida, Y. Fujita, “p-ZnO/n-ZnO Nanoparticles based UV Light Emitting Diodes.” JSAP spring meeting, 2020, **Poster presentation** (Abstract no- 15a-PA5-2).
4. **Islam Mohammad Shafiqul**, K. Odawara, M. F. B. Ahmad, J. Lin, T. Yoshida, Y. Fujita, “UV Electroluminescence from ZnO Nanoparticles based p-ZnO/n-ZnO homojunction LEDs.” JSAP spring meeting 2018, **Poster presentation** (Abstract no- 19p-P11-29).



List of other Conference Presentation (Co-Author):

1. Raj Deep, **Islam Mohammad Shafiqul**, Akazawa Takuma, Toshiyuki Yoshida, Yasuhisa Fujita: “Peak shift and Temperature effects in ZnO nanoparticles-based solution-processed LEDs”. The JSAP 69th Spring Meeting (2022) (abstract- 25a-E202-4).
2. Raj Deep, Yuki Konishi, **Islam Mohammad Shafiqul**, Jie Lin, Toshiyuki Yoshida, Yasuhisa Fujita: “Leakage current reduction in ZnO nanoparticle based near UV-LEDs”, The JSAP Autumn Meeting (2020).
3. Raj Deep, Atsuya Tabuchi, Yuki Konishi, **Islam Mohammad Shafiqul**, Jie Lin, Toshiyuki Yoshida, Yasuhisa Fujita: “Enhancing power of ZnO nanoparticle LEDs using silica coated silver Nano-particles”, The JSAP Spring Meeting (2020).
4. Yuki Konishi, Atsuya Tabuchi, **Islam Mohammad Shafiqul**, Jie Lin, Toshiyuki Yoshida, Yasuhisa Fujita, “Fabrication of large area light emitting devices by ZnO nanoparticle based near UV light emitting diodes”, International Symposium for Advanced Materials Research 2019 (ISAMR 2019), GIS Kaohsiung Asia’s New Bay Area Convention Center, Taiwan (2019).
5. Atsuya Tabuchi, **Islam Mohammad Shafiqul**, Jie Lin, Toshiyuki Yoshida, Yasuhisa Fujita, “Improvement of efficiency of ZnO nanoparticle LEDs by localized surface plasmon resonance”, The JSAP Autumn Meeting, (2019).
6. Yasuhisa Fujita, **Islam Mohammad Shafiqul**, Jie Lin, Toshiyuki Yoshida "The Effect of hole transporting layer in ZnO Nanoparticle LED." JSAP 2017, 8a-PA4-3.

Acknowledgments

First, I would like to express my most incredible gratitude to my honorable supervisor Professor Dr. Yasuhisa Fujita. It is an honor for me to thank him for the opportunities he gave me this study. I extend my inner thanks for his endless patience and great support. I wish to express my gratitude to Assistant Professor Dr. Toshiyuki Yoshida for his support and encouragement. They have created an environment where everyone is free to explore their research projects yet is always willing to give suggestions and advice. I also would like to thank the former and present members of Fujita-Yoshida laboratory, who have timely assisted whenever asked and for their fruitful cooperation. They all gave me good suggestions and opportunities to discuss scientific topics.

I would like to thank Dr. Jie Lin for sharing her vast knowledge and continuous support. I would also like to thank all members of SNCC Co., Ltd.

I would like to thank the cooperation of the Centre for Integrated Research in Science, Shimane University, for providing XRD and FE-SEM analysis.

I would like to thank for partially supporting by MEXT of Japan City Area Program of Shinji Lake & Nakaumi (2009-2012), JSPS KAKENHI Grant Number 25630150, The Canon Foundation, and S-Nanotech Co-Creation Co., Ltd.

Finally, I would like to thank my assistant supervisor, Professor Dr. Yasuji Yamada, Professor Dr. Ryo Sasai, and Associate Professor Dr. Wenchang Yeh for their invaluable suggestions and help.